Self-assembly and plasticity of synaptic domains through a reaction-diffusion mechanism

Christoph A. Haselwandter, Mehran Kardar, Antoine Triller, and Rava Azeredo da Silveira

Phys. Rev. E **92**, 032705 — Published 3 September 2015

DOI: 10.1103/PhysRevE.92.032705

Self-assembly and plasticity of synaptic domains through a reaction-diffusion mechanism

Christoph A. Haselwandter,[1,*] Mehran Kardar,[2,†] Antoine Triller,[3,‡] and Rava Azeredo da Silveira[4,5,§]

[1] *Departments of Physics & Astronomy and Biological Sciences, University of Southern California, Los Angeles, CA 90089, USA*
[2] *Department of Physics, Massachusetts Institute of Technology, Cambridge, MA 02139, USA*
[3] *IBENS, Institute of Biology at Ecole Normale Supérieure, Inserm U1024, CNRS UMR5197, 46 rue d'Ulm, 75005 Paris, France*
[4] *Department of Physics, Ecole Normale Supérieure, 24 rue Lhomond, 75005 Paris, France*
[5] *Laboratoire de Physique Statistique, Centre National de la Recherche Scientifique, Université Pierre et Marie Curie, Université Denis Diderot, France*

Signal transmission across chemical synapses relies crucially on neurotransmitter receptor molecules, concentrated in postsynaptic membrane domains along with scaffold and other postsynaptic molecules. The strength of the transmitted signal depends on the number of receptor molecules in postsynaptic domains, and activity-induced variation in the receptor number is one of the mechanisms of postsynaptic plasticity. Recent experiments have demonstrated that the reaction and diffusion properties of receptors and scaffolds at the membrane, alone, yield spontaneous formation of receptor-scaffold domains of the stable characteristic size observed in neurons. On the basis of these experiments we develop a model describing synaptic receptor domains in terms of the underlying reaction-diffusion processes. Our model predicts that the spontaneous formation of receptor-scaffold domains of the stable characteristic size observed in experiments depends on a few key reactions between receptors and scaffolds. Furthermore, our model suggests novel mechanisms for the alignment of pre- and postsynaptic domains and for short-term postsynaptic plasticity in receptor number. We predict that synaptic receptor domains localize in membrane regions with an increased receptor diffusion coefficient or a decreased scaffold diffusion coefficient. Similarly, we find that activity-dependent increases or decreases in receptor or scaffold diffusion yield a transient increase in the number of receptor molecules concentrated in postsynaptic domains. Thus, the proposed reaction-diffusion model puts forth a coherent set of biophysical mechanisms for the formation, stability, and plasticity of molecular domains on the postsynaptic membrane.

PACS numbers: 87.16.-b, 82.40.-g, 87.19.lp, 87.19.lw

I. INTRODUCTION

Synapses are asymmetric contact regions between neurons which mediate signal transmission from pre- to postsynaptic cells. It is thought [1] that the stability and plasticity of synapses constitute part of the physiological basis for memory formation and learning. One of the key regulators of signal transmission across chemical synapses are receptor molecules [1–4] concentrated in postsynaptic membrane domains opposite presynaptic terminals. Synaptic receptor molecules transiently bind to neurotransmitter molecules released by the presynaptic cell. The strength of the transmitted signal—the so-called postsynaptic potential—depends on the number of receptor molecules present in the postsynaptic domain [1, 3], and activity-induced variation in the concentration of synaptic receptors is one of the mechanisms governing postsynaptic plasticity [5–7]. A fundamental question in neurobiology is: What determines the number of receptor molecules in a postsynaptic domain? And an even more basic question is: Why do synaptic receptors concentrate at synapses rather than spread homogeneously on the cell membrane through diffusion?

An important role in the localization of receptors at synapses is played by scaffold molecules [1–4] which are thought to stabilize receptor molecules in synaptic membrane domains. Yet, recent experiments have demonstrated [7, 8] a rapid turnover of synaptic receptors [9–11] as well as their associated scaffolds [12–15], with individual molecules leaving and entering the synaptic domain on typical time scales as short as seconds. But the synaptic strength, which depends crucially on the number of receptor molecules concentrated in the postsynaptic domain, can be stable over months or even longer periods of time [16, 17]. Thus, the time scales of the synapse as a whole and its constitutive elements are not commensurate [8–10], and the question arises of how the measured molecular turnover and diffusion rates can be reconciled with the presence of stable synaptic receptor domains of the well-defined characteristic size observed in experiments. This is a particular instance of the general problem, pointed out many years ago [18], of how the physiological stability necessary for memory formation is achieved in the presence of the erratic dynamics that rule the molecular realm.

*Electronic address: cah77@usc.edu
†Electronic address: kardar@mit.edu
‡Electronic address: antoine.triller@ens.fr
§Electronic address: rava@ens.fr

What are the minimal conditions sufficient for the formation of receptor domains of a well-defined and stable characteristic size? From a theoretical perspective, it has been demonstrated [19] that cooperative interactions between receptors, which favor the insertion of new receptors into membrane regions with a high receptor density, can (transiently) stabilize pre-existing receptor clusters, while still allowing for a rapid turnover of individual receptors. A more recent, thermodynamic model [20] includes both receptor and scaffold molecules; it assumes that pre- and postsynaptic interactions stabilize scaffold molecules in certain pre-determined regions of the cell membrane, resulting in phase separation with a high receptor density opposite the presynaptic terminals and a relatively small density of receptors away from presynaptic contacts. Alternative dynamical models [21, 22] balance currents of receptors into and out of synaptic domains. The stability of synaptic domains then follows from an inward current sufficient to compensate for receptor depletion. Stabilization of receptor clusters has also been studied [23, 24] using models which rely on an interplay between spatial heterogeneity in receptor recycling and diffusive trapping of receptors in pre-existing synaptic domains. This has allowed quantitative description of single-molecule data on receptor diffusion in nerve cells, and suggested mechanisms for activity-dependent regulation of receptor number through local changes in receptor recycling.

From an experimental point of view, minimal systems devoid of the molecular machinery commonly associated with postsynaptic domain formation [25] have been used to study the conditions sufficient for the formation of receptor domains of a well-defined and stable characteristic size. In particular, single non-neural (fibroblast) cells were transfected with neuronal receptor and scaffold molecules [14, 26], allowing for the rapid diffusion of receptors [14, 27, 28] observed in neurons [8–10] as well as for interactions between receptors and scaffolds. If receptor and scaffold molecules were both present, receptor-scaffold domains (RSDs) formed spontaneously [14, 29–36]. Furthermore, RSDs were observed to be stable once they reached a characteristic size comparable to that of synaptic domains in neurons [14, 26, 29, 37]. If only receptors but no scaffolds were transfected, receptor domains did not emerge, apart from possible occurrences of transient micro-domains [26, 27]. If only scaffolds but no receptors were transfected, large intracellular blobs of scaffolds were observed, but no association with the cell membrane was detected [26, 38]. Collectively, these observations suggest [29] that receptor-scaffold interactions, together with the diffusion properties of each molecular species at the membrane, are sufficient for the formation, stability, and characteristic size of synaptic receptor domains. In particular, the presence of a presynaptic terminal is not essential for the occurrence of stable RSDs.

In this article, we build on the above experimental observations and our earlier theoretical work [29] to develop a comprehensive model of synaptic domains in terms of the underlying reaction and diffusion properties of receptor and scaffold molecules. Our article is organized as follows. We first discuss qualitative aspects of the spontaneous formation of stable synaptic receptor domains from a reaction-diffusion mechanism. This qualitative scenario is then translated into a mathematical description of the reaction and diffusion processes exhibited by receptors and scaffolds at the membrane. The mathematical formulation of our reaction-diffusion model yields constraints on the reaction and diffusion rates of receptors and scaffolds, which must be satisfied for the formation of stable synaptic receptor domains to occur. We then describe the results of computer simulations of our reaction-diffusion model, which allow us to make direct comparisons between patterns obtained from our model and the corresponding experimental patterns of RSDs. This is followed by a discussion of how, based on the reaction-diffusion model of synaptic receptor domains, local modifications in the receptor or scaffold diffusion rate induced by synaptic activity may yield alignment of pre- and postsynaptic domains. Furthermore, we show that the reaction-diffusion model of synaptic receptor domains suggests a biophysical mechanism of short-term postsynaptic plasticity in the number of receptors contained in an RSD. We conclude by summarizing our approach, discussing our predictions in light of experimental observations, and describing open questions pertaining to our model. The mathematical details of our reaction-diffusion model are presented in the appendix, along with a description of our numerical methods and possible generalizations of the reaction-diffusion model of synaptic receptor domains.

II. SPONTANEOUS FORMATION OF STABLE SYNAPTIC RECEPTOR DOMAINS

Before describing our quantitative results, we summarize here qualitative aspects of our mathematical model. Postsynaptic domains containing neurotransmitter receptors are enormously complex molecular assemblies involving thousands of proteins [2, 4, 8, 10]. Instead of considering the postsynaptic apparatus in its full complexity, we focus here on a minimal experimental system which was shown previously [29] to contain the components sufficient for the spontaneous formation of stable synaptic receptor domains of the characteristic size observed in neurons [14, 26, 37]. In this minimal experimental system, fibroblast cells were transfected with glycine receptors, which are one of the main receptor types at inhibitory synapses, and their associated scaffolds, gephyrin molecules. Accordingly, our model includes receptor molecules and their associated scaffolds, together with the reaction and diffusion properties of these molecules at the cell membrane (see Fig. 1(a)).

We assume that the membrane geometry is locally flat at the scale of synaptic receptor domains. This is a good approximation for synaptic receptor domains in fibrob-

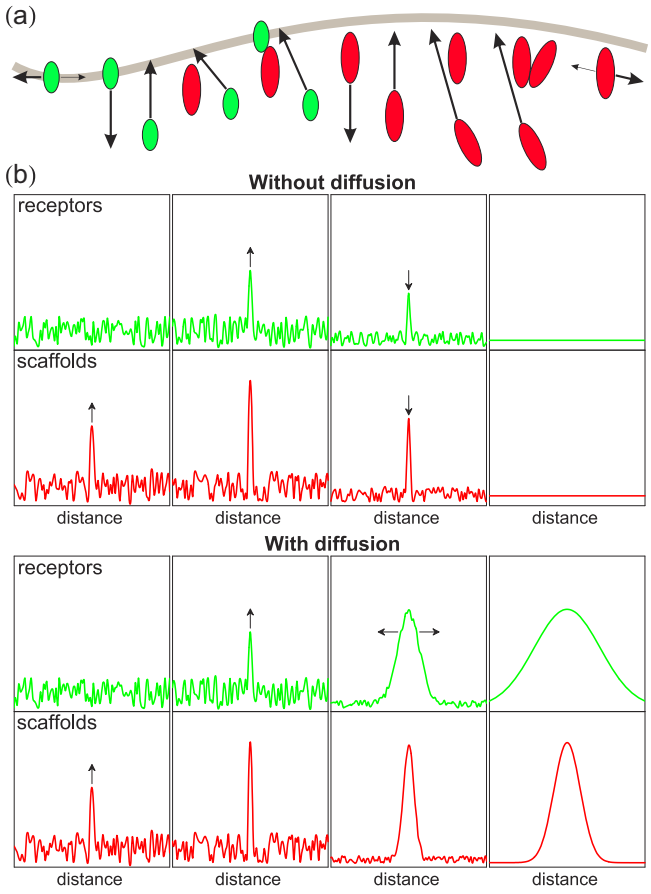

FIG. 1: (Color online) Reaction-diffusion mechanism for the formation and stability of synaptic receptor domains. (a) Schematic illustration of reactions between receptor (green) and scaffold (red) molecules, and the diffusion of receptors and scaffolds along the cell membrane (grey curve). Compared to free diffusion (thick arrows), diffusion in crowded membrane regions is hampered by steric constraints (thin arrows). The illustrated reactions correspond to endocytosis and insertion of receptors and scaffolds, as well as stabilization of receptors and scaffolds by scaffold molecules at the membrane. Molecular complexes formed by receptors and scaffolds are assumed to be transient [7–15]. See Sec. III for the mathematical expression of the indicated reaction and diffusion processes. (b) Illustration of the reaction-diffusion mechanism producing stable RSDs. Time evolution of receptor and scaffold concentrations in the absence of diffusion (top panels) and in the presence of diffusion (bottom panels) according to the mean-field reaction-diffusion model, which neglects noise in the reaction and diffusion of molecules.

last cells, but membrane curvature can be expected to introduce further complications in highly curved regions of neural membranes, e.g., in dendritic spines. We use the quantitative experimental data available for glycine receptors and gephyrin scaffolds [3, 9–11, 14, 27] as the basis for our numerical calculations. Thus, while our qualitative predictions may be generic to the self-assembly of synaptic receptor domains, our quantitative results pertain to glycine receptors and gephyrin scaffolds. Our model for the formation of stable RSDs relies crucially on the difference between the diffusivity of receptors and that of scaffolds, and on the property of scaffolds to stabilize other scaffolds as well as receptors at the membrane. Indeed, experiments on the diffusion properties of glycine receptors and gephyrin scaffolds [3, 9–11, 14, 27] suggest that receptors diffuse much more rapidly than scaffolds, while gephyrin scaffolds transiently bind [3, 9–11, 14, 27] other scaffold as well as receptor molecules (Fig. 1(a)).

Figure 1(b) illustrates the reaction-diffusion (Turing [39]) mechanism which yields [29], in our model, the spontaneous formation of synaptic receptor domains of a stable characteristic size. In the terminology of the reaction-diffusion mechanism of pattern formation [39–47], receptors play the role of 'inhibitors' of molecular concentrations in our model, while scaffolds play the role of 'activators.' In particular, we assume that receptors diffuse rapidly and inhibit increased molecular concentrations through steric constraints [8–10, 14, 27, 28], and that scaffolds diffuse slowly compared to receptors and activate increased molecular concentrations through transient binding to receptors as well as scaffolds [7–15].

Consider a random spatial fluctuation in the initial molecular concentrations of receptors and scaffolds, that produces a local excess of scaffolds (Fig. 1(b)). When this occurs, additional molecules of both species are further recruited at that membrane location because scaffolds activate increased molecular concentrations of both receptors and scaffolds. Now, if receptors diffuse away faster than scaffolds, the concentration of scaffolds initially wins over that of receptors in the perturbed region. As a result, the receptor and scaffold concentrations both increase in this region of the membrane, again because scaffolds are activators, and the scaffold concentration is further enhanced after diffusion. Eventually, however, this positive feedback is damped and a dynamic steady state is reached when a large diffusive current of receptors balances out the effective attraction of receptors and scaffolds into RSDs. This leads to the overall stability of RSDs in the presence of rapid molecular turnover and diffusion at the cell membrane [9–11, 27, 30]. Once the system reaches a steady state, the concentration profiles of receptor and scaffold molecules are inhomogeneous in space, i.e., there is spatial patterning. A key point, here, is that in the absence of rapid receptor diffusion the positive feedback responsible for the patterning instability is absent. Random perturbations then simply decay, and the steady state concentrations of receptors and scaffolds are homogeneous in space.

As just outlined, RSDs arise in our model because of the combined 'activator' nature of scaffold molecules, which stabilize themselves and receptors at the membrane, and 'inhibitor' nature of receptors, due to their steric repulsion. These features of the two molecular species, together with their diffusion properties, result in a patterning instability. One may wonder whether a converse scheme, in which scaffolds play the role of inhibitors and receptors play the role of activators, may

yield another candidate model; we discuss this possibility in some detail below, in Sec. V C.

III. REACTION-DIFFUSION MODEL OF SYNAPTIC RECEPTOR DOMAINS

A. Receptor and scaffold diffusion

Based on the experimental phenomenology of RSDs [3, 9–14, 27] we formulate a simple continuum model of RSDs [29] which incorporates receptor-receptor, receptor-scaffold, and scaffold-scaffold interactions, as well as the lateral diffusion of both molecular species on the cell membrane (Fig. 1(a)). We represent the local concentrations of receptor and scaffold molecules by the functions $r(x,y,t)$ and $s(x,y,t)$, where the variables x and y denote coordinates along the cell membrane, and the variable t denotes time. The movement and insertion of receptors and scaffolds is inhibited by steric repulsion [3, 9–11], which counteracts high molecular concentrations of receptors or scaffolds. For instance, single-molecule experiments have suggested [9, 10] that steric repulsive interactions yield nonlinear diffusion of receptors inside synaptic receptor domains, while receptors are able to diffuse freely outside synaptic domains. In order to account for such crowding effects in our coarse-grained model, we impose the constraint $0 \leq r+s \leq 1$ on all reaction and diffusion processes, where we have normalized r and s so that the maximum concentration of receptors and scaffolds is equal to 1. This steric constraint then yields the generalized reaction-diffusion equations

$$\frac{\partial r}{\partial t} = F(r,s) - \nu_r \nabla \cdot \mathbf{J}_r \,, \tag{1}$$

$$\frac{\partial s}{\partial t} = G(r,s) - \nu_s \nabla \cdot \mathbf{J}_s \,, \tag{2}$$

where the polynomials $F(r,s)$ and $G(r,s)$ describe the reactions in our system, and the diffusion currents read

$$\mathbf{J}_r = -D_r(1-s)\nabla r - D_r r \nabla s - (1-r-s) r \nabla D_r \,, \tag{3}$$

$$\mathbf{J}_s = -D_s(1-r)\nabla s - D_s s \nabla r - (1-r-s) s \nabla D_s \,. \tag{4}$$

The coefficients ν_r and ν_s in Eqs. (1) and (2) are the diffusion constants associated with receptors and scaffolds moving freely outside of RSDs [8–10], and $D_r(x,y,t)$ and $D_s(x,y,t)$ account for spatial and temporal variations in the receptor or scaffold diffusion rates [3, 48–55]. Experimental studies [3, 9–11, 13, 14, 27] of the diffusion properties of glycine receptors and gephyrin scaffolds, as well as of other types of receptors and scaffolds, suggest that $\nu_r \gg \nu_s$.

The non-standard diffusion terms in the generalized reaction-diffusion model in Eqs. (1) and (2) can be derived from a lattice gas formulation [56–58] of receptor and scaffold diffusion processes. In Appendix A we provide such a systematic derivation of Eqs. (1) and (2). Descriptions of multi-species diffusion under steric constraints of the form in Eqs. (3) and (4) have been used before in the context of population biology [56–58] and were found to yield the correct continuum description of the underlying lattice gas model. Here, for the purposes of the present discussion, we illustrate the way in which such equations can be derived heuristically and mention physical interpretations in the context of receptor and scaffold diffusion [29]. If we discretize space according to a mesh size a, the right-ward receptor current along the x-axis direction is proportional to

$$D_r(x,y)\, r(x,y)\, [1 - r(x+a,y) - s(x+a,y)] \,. \tag{5}$$

Similarly, the left-ward receptor current along the x-axis direction is proportional to

$$-D_r(x+a,y)\, r(x+a,y)\, [1 - r(x,y) - s(x,y)] \,. \tag{6}$$

To first order in a, the total current is then proportional to

$$-D_r \frac{\partial r}{\partial x}(1-s) - D_r r \frac{\partial s}{\partial x} - \frac{\partial D_r}{\partial x} r\,(1-r-s) \,, \tag{7}$$

which amounts to the x-component of Eq. (3). Thus, the first term in Eq. (3), $-D_r(1-s)\nabla r$, represents the combined effects of standard surface diffusion, biased in the direction of decreasing r, and of the excluded-volume mechanism, which limits diffusion in the direction of increasing s. Similarly, the current $-D_r r \nabla s$ is in the direction in which s is decreasing and arises because, due to the exclusion condition, it is favorable for receptor molecules to diffuse into regions with fewer scaffold molecules. These nonlinear corrections to the standard receptor diffusion current, $-\nabla r$, in Eq. (3) are important in regions with substantial scaffold concentrations, and provide a simple mean-field description of the observed steric effects on receptor diffusion inside RSDs [9, 10]. Finally, the current $-(1-r-s) r \nabla D_r$ is in the direction of decreasing D_r and is generated because membrane regions where D_r is reduced represent 'sinks' of the diffusive motion of receptors. Similar considerations hold for $\mathbf{J}_s$ in Eq. (4), which accounts for steric constraints on the diffusion of scaffolds inside RSDs. In principle, the reaction-diffusion mechanism for pattern formation [39–47] does not rely on steric repulsion or spatiotemporal variations in the diffusion rates, but we include these generalizations in our description of synaptic receptor domains in order to allow for the crowded membrane environment of RSDs [3, 9–11] and for putative effects of synaptic activity on receptor or scaffold diffusion [3, 48–55].

B. Receptor and scaffold interactions

What are suitable representations of the receptor and scaffold reaction kinetics in the reaction-diffusion model in Eqs. (1) and (2)? Even in our minimal model system for receptor domain formation, which does not in-

clude most of the synaptic machinery, molecular interactions are highly complex [3, 8–11]. For instance, receptors may be inserted into the cell membrane as receptor-scaffold complexes and, conversely, receptors may diffuse on the cell membrane while bound to scaffold molecules. Here, our aim is to formulate simple reaction kinetics between receptors and scaffolds which are consistent with the basic biochemistry of glycine receptors and gephyrin scaffolds [3, 4, 9–11], and which capture the interactions essential for the formation and stability of RSDs (Fig. 1(a)). We therefore only consider the fields r and s describing the concentrations of receptors and scaffolds at the membrane. While our model allows for transient complexes of receptors and scaffolds, it does not consider stable complexes of receptors and scaffolds. The latter would necessitate additional fields capturing the concentrations of stable bound complexes at the membrane, and corresponding parameter sets describing the reaction and diffusion properties of stable complexes. At the cost of introducing additional reaction and diffusion parameters, our model could be extended to allow for such stable higher-order complexes (see Appendix D).

On the most basic level, receptors and scaffolds may both be removed from the cell membrane through endocytosis or some other molecular process [3, 9, 10], yielding reactions of the form $R \longrightarrow R_b$ and $S \longrightarrow S_b$. In these expressions, R and S stand for receptors and scaffolds at the membrane, while R_b and S_b denote receptors and scaffolds in the cytoplasmic 'bulk' of the cell. Using the standard formalism of chemical dynamics [40–47], these reactions are represented in Eqs. (1) and (2) by the terms

$$F_1 = -f_1 r\,, \tag{8}$$

$$G_1 = -g_1 s\,, \tag{9}$$

in F and G, respectively, where f_1 and g_1 are effective parameters describing the reaction rates associated with the decay of receptor and scaffold populations at the membrane. While previous studies have allowed for spatial variations in the rates of receptor recycling [23, 24], we assume, here, for the sake of simplicity, that reaction rates are constant along the cell membrane.

The reactions in Eqs. (8) and (9) involve only single receptors or scaffolds, but interactions between receptors and scaffolds are crucial for the formation of stable RSDs in experiments [26, 27, 29, 38]. Thus, we must augment Eqs. (8) and (9) to allow for nonlinear reaction terms in Eqs. (1) and (2). In particular, glycine receptors transiently bind to gephyrin scaffolds. It has been argued [3, 9–11] that this reaction is paramount for the preferential accumulation of glycine receptors in RSDs. In our coarse-grained reaction-diffusion model, the simplest expression of receptor stabilization through scaffolds is provided by the reaction $R_b + S \longrightarrow R + S$, which corresponds to the preferential insertion of receptors into membrane regions with an increased scaffold population [9, 10]. Following the same procedure [40–47] as above, this reaction yields the contribution

$$F_2 = f_2(1 - r - s)s \tag{10}$$

to F in Eq. (1), where f_2 is the rate associated with the reaction $R_b + S \longrightarrow R + S$ and the factor $1 - r - s$ imposes the steric constraint $0 \leq r + s \leq 1$. Similarly, on the basis of structural models of gephyrin scaffolds it has been suggested [3, 9] that gephyrin molecules can form dimers as well as trimers, possibly yielding a honeycomb lattice of gephyrin in synaptic membrane domains. In our model, a simple representation of the transient dimerization and trimerization of scaffolds is obtained by including the reactions $S_b + S \longrightarrow 2S$ and $S_b + 2S \longrightarrow 3S$. These reactions yield [40–47] the contributions

$$G_2 = g_2(1 - r - s)s\,, \tag{11}$$

$$G_3 = g_3(1 - r - s)s^2 \tag{12}$$

to G in Eq. (2), where g_2 and g_3 are the corresponding reaction rates and, as in Eq. (10), the factor $1 - r - s$ enforces the steric constraint $0 \leq r + s \leq 1$.

We show, below, that the sums of the reactions in Eqs. (8)–(12) constitute a simple reaction scheme yielding RSDs, and we term this reaction scheme *model A*. It is mathematically convenient to redefine the reaction rates in Eq. (8)–(12) to write the reaction terms F and G in Eqs. (1) and (2) associated with model A as

$$F_A(r,s) = -b\left(r - \frac{s}{\bar{s}}E\bar{r}\right)\,, \tag{13}$$

$$G_A(r,s) = -\beta\,(s - sE) + \mu\frac{s}{\bar{s}}E\,(s - \bar{s})\,, \tag{14}$$

where b, β, and μ are constants with $\beta > \mu$, $E = \frac{1-r-s}{1-\bar{r}-\bar{s}}$ imposes the steric exclusion constraint $0 \leq r+s \leq 1$, and the concentrations $(r,s) = (\bar{r},\bar{s})$ are non-trivial solutions of the homogeneous fixed point equations

$$F(\bar{r},\bar{s}) = G(\bar{r},\bar{s}) = 0\,, \tag{15}$$

with $\bar{r} \neq 0, 1$ and $\bar{s} \neq 0, 1$. Note that Eqs. (8)–(12) and Eqs. (13) and (14) contain the same number of parameters, but Eqs. (13) and (14) yield the fixed point solution $(r,s) = (\bar{r},\bar{s})$ in a transparent manner. As explained in Appendix B, the reaction kinetics in Eqs. (13) and (14) can, in addition to the phenomenological argument given above, also be motivated from the mathematical properties of reaction-diffusion instabilities.

While model A provides a simple phenomenological description of a few elementary interactions between glycine receptors and gephyrin scaffolds, other molecular interactions occur in general. Such additional interactions between receptors and scaffolds can be included following similar steps as above and, in order to ascertain the effect of different reaction schemes on the dynamics of RSDs, we survey here a set of different models of varying levels of complexity (see Table I). In particular, a simple modification of the reaction kinetics of model A is implemented in *model A′* which, in addition to the reactions incorporated in model A, allows for higher-order reactions in F in Eq. (1) up to the same order as G. Conversely, *model B* contains the same receptor reaction kinetics as

TABLE I: Reaction schemes for synaptic receptors and scaffolds. Chemical reactions are expressed in terms of R and S, which stand for receptors and scaffolds at the membrane, R_b and S_b, which denote receptors and scaffolds in the bulk of the cell, and the unspecified bulk molecule M_b, which may be a receptor molecule, a scaffold molecule, or some other molecule interacting with receptors or scaffolds at the membrane. All molecular complexes are assumed to be only transient [7–15].

	Contributions to F	Contributions to G
Model A	$R \longrightarrow R_b\,,\ R_b + S \longrightarrow R + S$	$S \longrightarrow S_b\,,\ S_b + S \longrightarrow 2S\,,\ S_b + 2S \longrightarrow 3S$
Model B	$R \longrightarrow R_b\,,\ R_b + S \longrightarrow R + S$	$S \longrightarrow S_b\,,\ S_b + 2S \longrightarrow 3S$
Model A$'$	$R \longrightarrow R_b\,,\ R_b + S \longrightarrow R + S\,,\ R_b + R + S \longrightarrow 2R + S$	$S \longrightarrow S_b\,,\ S_b + S \longrightarrow 2S\,,\ S_b + 2S \longrightarrow 3S$
Model B$'$	$R \longrightarrow R_b\,, R_b + S \longrightarrow R + S\,,\ R_b + R + S \longrightarrow 2R + S$	$S \longrightarrow S_b\,,\ S_b \longrightarrow S\,,\ S_b + 2S \longrightarrow 3S$
Model C	$R \longrightarrow R_b\,,\ R_b \longrightarrow R\,,\ M_b + R \longrightarrow R_b + M_b\,,$ $R_b + S \longrightarrow R + S\,,\ R_b + R + S \longrightarrow 2R + S$	$S \longrightarrow S_b\,,\ S_b \longrightarrow S\,,\ M_b + S \longrightarrow M_b + S_b\,,$ $S_b + 2S \longrightarrow 3S$

model A, but fewer lower-order interactions in the scaffold reaction kinetics and, in particular, does not allow for dimerization of scaffolds. Model B allows us to test whether dimerization of scaffolds is essential for RSDs. In analogy to model A$'$, *model B$'$* extends the reaction kinetics of model B so that F and G in Eqs. (1) and (2) contain reactions of the same order. Finally, *model C* [29] represents the most complex reaction scheme considered here, and contains all the reactions included in models A, A$'$, B, and B$'$. Mathematical representations of the various reaction schemes in Table I are obtained following similar steps as for model A (see Appendix B).

C. Constraining the interaction and diffusion of receptors and scaffolds

In principle, reaction rates such as those in Eqs. (13) and (14), as well as the receptor and scaffold diffusion coefficients, can be estimated on the basis of single-molecule experiments. However, while great efforts have been expended [3, 8–11] on the quantitative characterization of the reaction and diffusion properties of glycine receptors and gephyrin scaffolds, as well as of other types of synaptic receptors and scaffolds, such measurements are difficult to carry out in the complex membrane environment provided by living cells. Our model provides a complementary approach for constraining the reaction and diffusion rates of receptors and scaffolds, which relies on the mathematical conditions mandated by the reaction-diffusion mechanism for domain formation [29, 39–47]. These mathematical conditions are expressed in terms of the linear stability matrix associated with Eqs. (1) and (2). In particular, for the zero Fourier (infinite wavelength) mode of our reaction-diffusion system only the reaction terms in Eqs. (1) and (2) contribute to the linear stability matrix, which can then be written as

$$\mathbf{M} = \begin{pmatrix} r_{11} & r_{12} \\ s_{21} & s_{22} \end{pmatrix} = \begin{pmatrix} \frac{\partial F}{\partial r} & \frac{\partial F}{\partial s} \\ \frac{\partial G}{\partial r} & \frac{\partial G}{\partial s} \end{pmatrix}\,, \tag{16}$$

with all terms evaluated at $(r, s) = (\bar{r}, \bar{s})$. For the reaction-diffusion model in Eqs. (1) and (2) to exhibit domain formation, instability must occur at a finite wavelength. Thus, the homogeneous non-trivial solution must be stable to uniform perturbations and, hence, the real parts of the eigenvalues of the stability matrix in Eq. (16) must be smaller than zero. It follows that the trace of the stability matrix is negative and the determinant is positive:

$$\mathrm{tr}\,\mathbf{M} < 0\,, \tag{17}$$

$$\det\mathbf{M} > 0\,. \tag{18}$$

Moreover, for Eqs. (1) and (2) to admit domain formation at a finite length scale, the real part of the larger eigenvalue associated with the linear stability matrix at $(r, s) = (\bar{r}, \bar{s})$ must pass through zero for some Fourier modes, yielding a finite (positive) characteristic length scale in the system. This means [29] that for certain Fourier modes the determinant of the stability matrix of Eqs. (1) and (2) vanishes, and we find

$$\begin{aligned} &\nu_r\left[(1-\bar{s})s_{22} - \bar{r}s_{21}\right] + \nu_s\left[(1-\bar{r})r_{11} - \bar{s}r_{12}\right] \\ &\quad > 2\left[\nu_r\nu_s(1-\bar{r}-\bar{s})\det\mathbf{M}\right]^{1/2}\,, \end{aligned} \tag{19}$$

where, for simplicity, we have set $D_r = D_s = 1$.

For a given choice of reaction kinetics, Eqs. (17) and (18) impose constraints on the relative values of the reaction rates, while Eq. (19) constrains the relative values of the reaction and diffusion rates. For instance, in model A we obtain

$$\mathbf{M} = \begin{pmatrix} -b\frac{1-\bar{s}}{1-\bar{r}-\bar{s}} & b\frac{\bar{r}}{\bar{s}}\left[1 - \frac{\bar{s}}{1-\bar{r}-\bar{s}}\right] \\ -\beta\frac{\bar{s}}{1-\bar{r}-\bar{s}} & \mu - \beta\frac{\bar{s}}{1-\bar{r}-\bar{s}} \end{pmatrix} \tag{20}$$

from Eq. (16) with Eqs. (13) and (14). We note that Eq. (20) implies that $r_{11} < 0$ and $s_{21} < 0$. Equations (17) and (18) then yield

$$b(1-\bar{s}) + \beta\bar{s} - \mu(1-\bar{r}-\bar{s}) > 0\,, \tag{21}$$

$$\beta(\bar{r}+\bar{s}) - \mu(1-\bar{s}) > 0\,. \tag{22}$$

These constraints, together with Eq. (19), must necessarily be satisfied by the reaction and diffusion rates of

model A for Eqs. (1) and (2) to exhibit domain formation through a reaction-diffusion mechanism. The corresponding constraints on the other formulations of the reaction kinetics in Table I are obtained from Eqs. (17)–(19) following similar steps.

IV. RESULTS

A. The reaction-diffusion mechanism produces stable synaptic receptor domains

In order to investigate the reaction-diffusion mechanism for the formation and stability of RSDs we simulated Eqs. (1) and (2) for a variety of different choices of the receptor and scaffold reaction and diffusion dynamics. Using reaction and diffusion rates within the ranges of values suggested by experiments [3, 9–11, 14, 27], we observed in our simulations the spontaneous formation of stable patterns of RSDs with a characteristic wavelength of approximately 1 μm (see Fig. 2). Furthermore, we obtained in our simulations a stable characteristic RSD area of 0.2 to 0.3 μm^2. Provided that the constraints in Eqs. (17)–(19) were satisfied, these results were robust with respect to perturbations to the reaction kinetics. The spontaneous formation, stability, and characteristic size of synaptic receptor domains found in our simulations are consistent with the corresponding experimental results [14, 26, 29, 37] on synaptic receptor domains in neurons and transfected non-neural cells.

While the spontaneous formation and stability of RSDs are generic features of our reaction-diffusion model, the detailed properties of the patterns of RSDs obtained in our simulations were dependent on the particular model formulation considered. We discuss first the most straightforward case of receptor and scaffold diffusion rates which are constant along the cell membrane, which corresponds to $D_r = D_s = 1$ in Eqs. (1) and (2). Figure 2(a) displays numerical solutions of Eqs. (1) and (2) with the reaction kinetics associated with model A in Table I, or Eqs. (13) and (14), at a time of 24 hours after initiation of pattern formation from random initial concentrations of receptors and scaffolds. In the steady state, we obtained regular (hexagonal) patterns of receptor and scaffold domains with a wavelength of approximately 1 μm. The receptor and scaffold patterns were in phase with each other and formed on a time scale of hours. Individual RSDs had an area of approximately 0.2 to 0.3 μm^2 and, once the pattern had formed, the size and location of RSDs was stable.

We note that the time scale of RSD formation in our simulations, which is of the order of hours, is significantly longer than the typical molecular time scales appearing in the reaction-diffusion model, which are of the order of seconds (see Appendix C for a discussion of the parameter values used in our simulations). The emergence of this longer time scale can be intuited along the lines of arguments used previously in the context of focal adhesions [59]. The formation of stable patterns of RSDs requires a redistribution of receptors and scaffolds through diffusion (Fig. 1(b)). Since scaffolds diffuse slower than receptors in our model, the time scale of RSD formation is set by the characteristic size of RSDs together with the scaffold diffusion coefficient, for which we use $\nu_s = (0.02\text{–}0.05) \times 10^{-2} \mu\text{m}^2/\text{s}$ in Fig. 2. Combining this range of scaffold diffusion coefficients with the characteristic wavelength, 1 μm, of patterns of RSDs in Fig. 2 yields a characteristic time scale $\sim$ 30–80 min, consistent with the time scale of RSD formation obtained in our simulations.

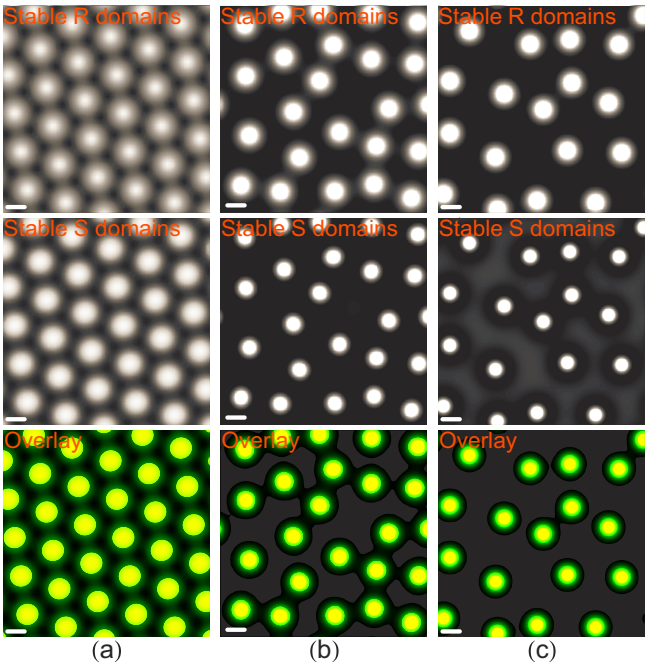

FIG. 2: (Color online) Stable patterns of synaptic receptor domains. Numerical solutions of Eqs. (1) and (2) with $D_r(x, y, t) = D_s(x, y, t) = 1$ for the reaction kinetics in (a) model A in Table I at time $t = 24$ hrs, (b) model B$'$ in Table I at time $t = 2$ hrs, and (c) model C in Table I at time $t = 24$ hrs. In our simulations, we used random initial conditions in the receptor and scaffold concentrations at time $t = 0$, and the generated patterns were found to be stable. The top panels show the receptor concentrations at the membrane, the middle panels display the scaffold concentrations at the membrane, and the lower panels were obtained by superimposing the receptor and scaffold concentrations in the top and middle panels (receptors in green, scaffolds in red, overlapping receptor and scaffold concentrations in yellow). For all reaction kinetics considered, receptor and scaffold domains are in phase with each other. Reaction and diffusion rates were chosen as specified in Eqs. (C6)–(C8) (see Appendix C for further details). Scale bars, 0.5 μm.

For model A$'$ in Table I we observed patterns which were similar to the results in Fig. 2(a), and also found the same characteristic size of RSDs. By contrast, with the reaction kinetics of model B in Table I, we were not able to obtain stable RSDs in our simulations; while model B

allows for a Turing instability, the resulting patterns of corrugated receptor and scaffold concentrations are out of phase, and thus no RSDs emerge. This can be intuited by noting that, in order to satisfy Eq. (18), we must have $s_{22} < 0$ in model B, which means that scaffolds do not stabilize other scaffolds around the homogeneous fixed point $(r, s) = (\bar{r}, \bar{s})$. In other words, our reaction-diffusion model suggests that to obtain RSDs, scaffolds need to be autocatalytic, which is in agreement with the basic phenomenology of gephyrin scaffolds [3, 9–11].

In contrast to model B, stable patterns of RSDs are readily obtained with the reaction kinetics corresponding to model B′ in Table I (see Fig. 2(b)). The size of RSDs produced by model B′ in our simulations was similar to that of the RSDs obtained with models A and A′. However, the large-scale patterns obtained with model B′ were more irregular than those produced by models A and A′. The irregularity of the patterns generated by model B′ is reminiscent of experimental results on patterns of RSDs [14, 29]. As shown in Fig. 2(c), irregular patterns of RSDs were also obtained with model C in Table I. As for models A, A′, and B′, RSDs formed spontaneously on a time scale of hours in model C, and the size of RSDs was stable once the patterns had formed. We found the irregular locations of the RSDs produced by models B′ and C to be stable over the time scales accessible to our simulations.

Depending on the model formulation used, the concentrations of receptors and scaffolds inside RSDs can be increased by factors of more than ≈ 18 and ≈ 11 or by as little as ≈ 1.3 and ≈ 4.2 over their respective molecular concentrations outside RSDs. For example, for model C in Fig. 2(c) receptor and scaffold concentrations increase by factors of ≈ 19 and ≈ 4.2. However, the numerical values of the relative receptor and scaffold concentrations inside and outside RSDs depend on the details of the reaction kinetics and, considering the uncertainties involved in experimental measurements of the reaction and diffusion parameters entering our model, do not represent general model predictions.

Akin to other types of reaction-diffusion models [40–47, 60, 61], our reaction-diffusion model of synaptic receptor domains predicts that receptor and scaffold molecules can produce a variety of different patterns depending on the specific diffusion rates considered. For instance, after varying the scaffold diffusion coefficient in model A, we observed the stable patterns shown in Fig. 3(a). The characteristic wavelength of these patterns was approximately 0.5 μm, and circular RSDs were now replaced by labyrinthine patterns of receptors and scaffolds which were out of phase. This suggests that experimental modification of the diffusion properties of scaffolds (or receptors) may influence the shape of stable domains in a manner that is, at least qualitatively, predictable.

We also observed in our simulations that, in contrast to variations in diffusion rates, the formation of RSDs is generally quite insensitive to variations in reaction rates. For instance, experiments suggest [3, 9, 10] characteristic

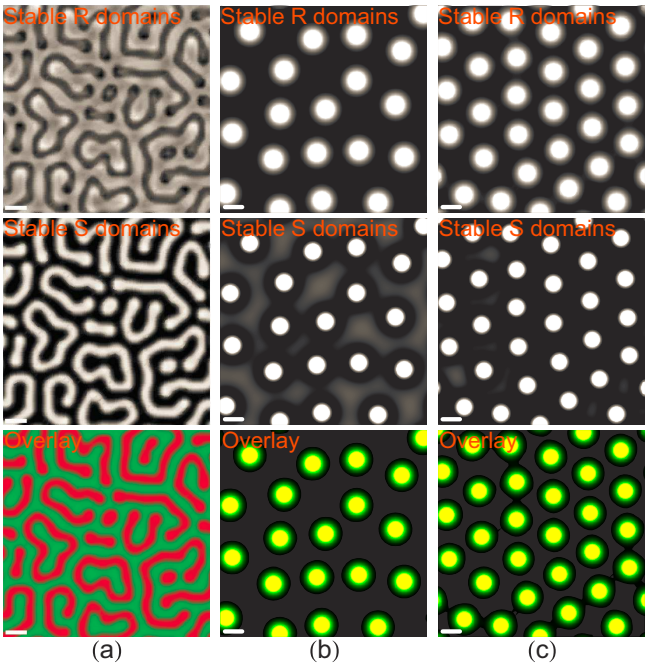

FIG. 3: (Color online) Perturbation of synaptic receptor domains. Numerical solutions of Eqs. (1) and (2) as in Fig. 2, for (a) model A in Table I at time $t = 2$ hrs and (b,c) model C in Table I at time $t = 24$ hrs. For the simulations in panel (a), the scaffold diffusion coefficient was decreased by a factor 0.2 compared to the scaffold diffusion coefficient used in Fig. 2(a), with all other parameter values remaining the same. For the simulations in panels (b) and (c), the rate of receptor endocytosis $R \longrightarrow R_b$ was decreased by a factor 10^{-3} compared to Fig. 2(c), with (b) the rates of $R_b \longrightarrow R$ and $M_b + R \longrightarrow M_b + R_b$ increased compared to Fig. 2(c), and (c) the same reaction rates as in Fig. 2(c) (with the exception of the rate of $R \longrightarrow R_b$), with all other parameter values remaining the same. The receptor and scaffold concentrations are out of phase in panel (a) but in phase in panels (b) and (c). Reaction and diffusion rates were chosen as specified in Eqs. (C9)–(C11) (see Appendix C for further details). Scale bar, 0.5 μm.

time scales for receptor turnover ranging from seconds to hours. As shown in Figs. 3(b) and 3(c), patterns comparable to those in Fig. 2 were obtained when the rate of endocytosis of receptor molecules was decreased by several orders of magnitude, from decay times of seconds to decay times of hours. Thus, we find that, if the reaction rates are chosen within the broad ranges of values suggested by experiments and constrained by Eqs. (17)–(19), our reaction-diffusion model can yield stable RSDs of the characteristic size observed in experiments. One caveat, here, is that the rates used in the model refer to molecular reactions, while the time scales obtained experimentally may be 'effective time scales' that result from the concatenation of several chemical reactions, and it is not straightforward to relate the two. We return to this issue in Sec. V.

B. The reaction-diffusion mechanism yields a characteristic size of synaptic receptor domains

The emergence of a characteristic size of RSDs in our simulations can be understood from the linear stability analysis of Eqs. (1) and (2) [29]. In particular, the two Fourier modes for which the larger eigenvalue associated with the linear stability matrix of Eqs. (1) and (2) at the homogeneous fixed point $(r, s) = (\bar{r}, \bar{s})$ vanishes define a band of unstable modes. A simple estimate of the characteristic wavelength of the patterns generated by Eqs. (1) and (2), and corresponding characteristic size of RSDs, is provided by the mid-point of the band of unstable modes, from which we find the characteristic scale

$$\ell_c = 2\pi \sqrt{\frac{2\nu_r \nu_s (1 - \bar{r} - \bar{s})}{\nu_r \left[(1 - \bar{s}) s_{22} - \bar{r} s_{21}\right] + \nu_s \left[(1 - \bar{r}) r_{11} - \bar{s} r_{12}\right]}}, \tag{23}$$

where, for the sake of simplicity, we have set $D_r = D_s = 1$. Note that the constraints in Eqs. (18) and (19) ensure that $\ell_c > 0$. The estimate in Eq. (23) is obtained by calculating the eigenvalues of the stability matrix associated with Eqs. (1) and (2) and, for the sake of simplicity, only allowing for non-zero Fourier modes in one spatial direction, which is equivalent to permitting diffusion in only one spatial direction in Eqs. (1) and (2). The eigenvalues of the stability matrix are functions of the square of the wavenumber. The two zeros of the larger eigenvalue yield expressions for the squares of two critical wavenumbers delineating the band of unstable modes, which we average, invert, take the square root of, and multiply by 2π to obtain Eq. (23). In agreement with our numerical results, Eq. (23) yields $\ell_c \approx 1$ μm for the parameter values used in Figs. 2, 3(b), and 3(c), and $\ell_c \approx 0.5$ μm for the parameter values used in Fig. 3(a).

In principle, Eq. (23) predicts the characteristic size of RSDs for a given set of reaction and diffusion rates measured in experiments. In practice, however, experiments have so far only been able to yield broad ranges for the rates of the reaction and diffusion processes exhibited by synaptic receptors and scaffolds. Moreover, Eqs. (17)–(19) only constrain the relative values of reaction and diffusion rates in the form of inequalities, leaving considerable freedom in the choice of reaction and diffusion rates for the various model formulations. Thus, the characteristic size of RSDs obtained in our simulations is not a model prediction but, rather, a consistency check that, for reaction and diffusion rates within the broad ranges suggested by experiments [3, 9–11, 14, 27], our model can indeed yield stable RSDs of the characteristic size found in experiments.

Equation (23) can be employed to make simple order-of-magnitude estimates of the characteristic scale of RSDs associated with different reaction and diffusion properties of receptors and scaffolds. For instance, the general expression in Eq. (23) can be simplified by noting that $\nu_r \gg \nu_s$. If we assume further that the homogeneous fixed point is such that $\bar{r} \ll 1$ and $\bar{s} \ll 1$, Eq. (23) is then approximated by $\ell_c \approx 2\pi\sqrt{2\nu_s/s_{22}}$. The magnitude of s_{22} in Eq. (16) is dominated by the fastest scaffold interactions, for which various experiments [3, 11] suggest $s_{22} \approx 10^{-2}$ s^{-1} (though this may correspond to an 'effective' rate combining several chemical reactions—see above and Sec. V). For a receptor diffusion coefficient $\nu_r \approx 10^{-2}$ μm^2 s^{-1} [3, 9–11, 14, 27], we then find that the characteristic size of RSDs varies from approximately 0.4 μm to 1 μm as ν_s varies from to $\nu_s \approx 0.01$ ν_r to $\nu_s \approx 0.1$ ν_r. These order-of-magnitude predictions of our model agree with experiments on RSDs formed by glycine receptors and gephyrin scaffolds [14, 26, 29, 37].

C. Alignment of pre- and postsynaptic domains through local modification of receptor or scaffold diffusion rate

Among the requirements for a mature synapse, perhaps the most basic one is that the pre- and postsynaptic domains face each other [1, 2]. If synaptic domains form and stabilize spontaneously, without any presynaptic involvement, what aligns pre- and postsynaptic domains? Most obviously, perhaps, membrane proteins, such as neurexin on the presynaptic side and neuroligin on the postsynaptic side, may provide mechanisms for the alignment of the two synaptic domains by way of chemical bonds [62]. Our approach suggests a complementary, biophysical mechanism for the alignment of synaptic domains which relies on local variations in the diffusion or reaction rates of receptor or scaffold molecules induced by neural activity. Indeed, it has been observed [3, 53–55] that the diffusion of receptors on the postsynaptic membrane can be modified through the binding of presynaptic neurotransmitter molecules. In addition, scaffold diffusion may be [48–52] decreased by interactions with neuroligin and further modulated by synaptic activity. As a simple phenomenological perturbation to the reaction-diffusion mechanism for the formation and stability of synaptic receptor domains, we implemented pre- and postsynaptic interactions through a local increase in the receptor diffusion rate, or a local decrease in the scaffold diffusion rate, and simulated our reaction-diffusion model with now varying $D_r(x, y, t)$ or $D_s(x, y, t)$ in Eqs. (1) and (2).

First we considered the case of a postsynaptic membrane on which RSDs had already formed, without presynaptic involvement. When sustained presynaptic activity, modelled by increased receptor diffusion, was turned on at localized spots (representing the postsynaptic membrane locations opposite presynaptic terminals), we found that RSDs slid on the postsynaptic membrane in order to align their centers to these spots, over a time scale of hours (Fig. 4(a)). We considered next the case in which sustained presynaptic stimulation occurred concomitantly with the emergence of RSDs: these then appeared preferentially across presynaptic terminals (Fig. 4(b)). In order to investigate the alignment mech-

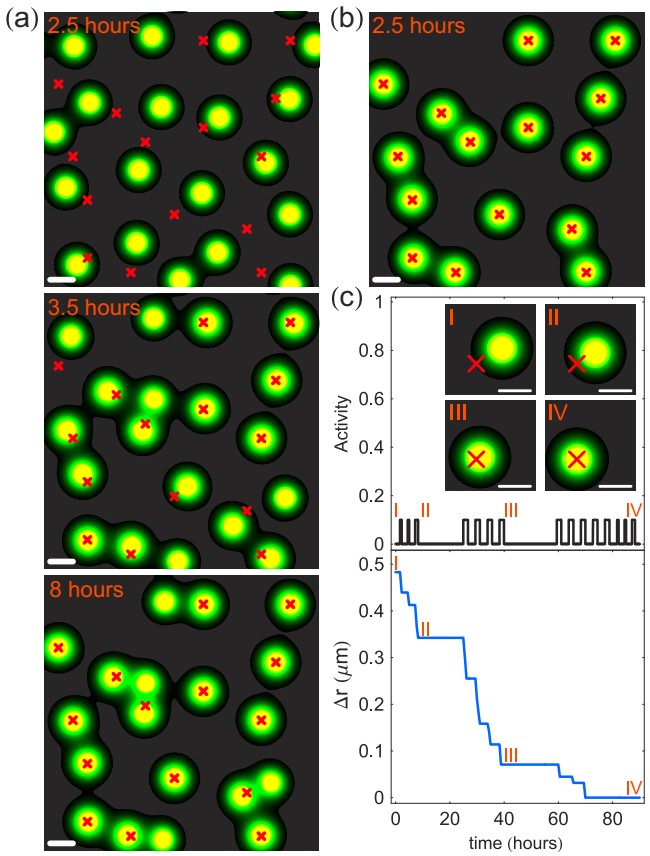

FIG. 4: (Color online) Alignment of postsynaptic domains with presynaptic domains through local variations in the diffusion rate. (a) Sustained synaptic activity is turned on at locations marked with a cross, after stable domains have already formed (at time $t = 2.7$ hrs). Over a time scale of hours, RSDs slide to match the locations of stimulation. (b) If stimulation is applied early in the formation of RSDs, these nucleate preferentially at locations of synaptic stimulation. (c) Response of a mature RSD to off-center pulses of synaptic activity. Top panel: temporal profile of on/off stimulation. Insets: Snapshots of RSD at selected times. Bottom panel: separation, Δr, between the location of maximal synaptic activity and the RSD center. The periods of activity in panel (c) lasted 2000 s, 4000 s, and 6000 s. All results were obtained by simulating Eqs. (1) and (2) with $D_s(x, y, t) = 1$ and a locally increased $D_r(x, y, t) > 1$ in the membrane regions marked by a cross, using the reaction kinetics of model C in Table I. Reaction and diffusion rates were chosen as specified in Eq. (C8) (see Appendix C for further details). Scale bar, 0.5 μm.

anism more closely, we submitted a RSD to repeated episodes of presynaptic activity from a terminal shifted in space with respect to the RSD. We found that each stimulation episode caused smooth sliding of the RSD toward the presynaptic terminal (Fig. 4(c)). According to the reaction-diffusion model of synaptic receptor domains (Fig. 1(b)), a local increase in the receptor diffusion rate such as considered in Fig. 4 has a similar effect as a local decrease in the scaffold diffusion rate. Indeed, we observed similar movements of RSDs as in Fig. 4 if the scaffold diffusion rate was locally decreased instead of the receptor diffusion rate increased. Conversely, we found that RSDs were repelled from regions with decreased receptor or increased scaffold diffusion rates, respectively.

The translation of RSDs shown in Fig. 4 has a simple qualitative explanation in terms of the receptor and scaffold molecule dynamics captured by our reaction-diffusion model: Enhanced receptor diffusion (or reduced scaffold diffusion) near the fringe of a domain (Fig. 4(c), top panel) yields a local increase in the scaffold molecule concentration (by the very same reaction-diffusion mechanism that governs RSD formation, illustrated in Fig. 1(b)) and, in turn, of receptor concentration. As a result, the RSD gradually shifts toward the stimulation spot. The reverse argument holds for repulsion of RSDs from membrane regions with reduced receptor diffusion (or enhanced scaffold diffusion). We also found in our simulations that, if receptor and scaffold diffusion rates were both locally modified by an equal fraction, RSDs were gradually drawn into regions with a decreased diffusion rate, and away from regions with an increased diffusion rate. But, in this case, the balance between inhibitors (receptor molecules) and activators (scaffold molecules) in our reaction-diffusion model was not disturbed by the modification of diffusion rates, and the (weak) localization of RSDs only resulted from the collective diffusion of RSDs into low diffusivity regions.

D. Postsynaptic plasticity mediated by receptor trafficking

The scenario for pre- and postsynaptic alignment described above suggests also a speculative mechanism for short-term postsynaptic plasticity. It is well known [5–7] that synaptic activity can lead to local variations in the postsynaptic receptor number, which is one of the mechanisms of postsynaptic plasticity. Short-term postsynaptic plasticity can result from one of a number of possible molecular processes. In particular, it has been proposed [63] that receptors are stabilized by an 'anchoring' protein molecule, and that the functional properties of individual receptors are modified upon binding with the protein. Furthermore, it has been found that activity-dependent changes in receptor currents into or out of synaptic domains [21, 22], or activity-dependent regulation of the local recycling rates of receptors [19, 23, 24], can yield shifts in the postsynaptic receptor number. Here, by contrast, we assume no such chemical changes, modification of net receptor currents, or local regulation of receptor recycling rates; short-term plasticity results [29] from the same biophysical instability which leads to self-assembly of domains together with the assumption that the diffusion rates of receptors or scaffolds can be locally modulated by synaptic activity. This assumption is supported by the experiments mentioned above [3, 7, 48–55], according to which synaptic stimulation may modify receptor or scaffold diffusion.

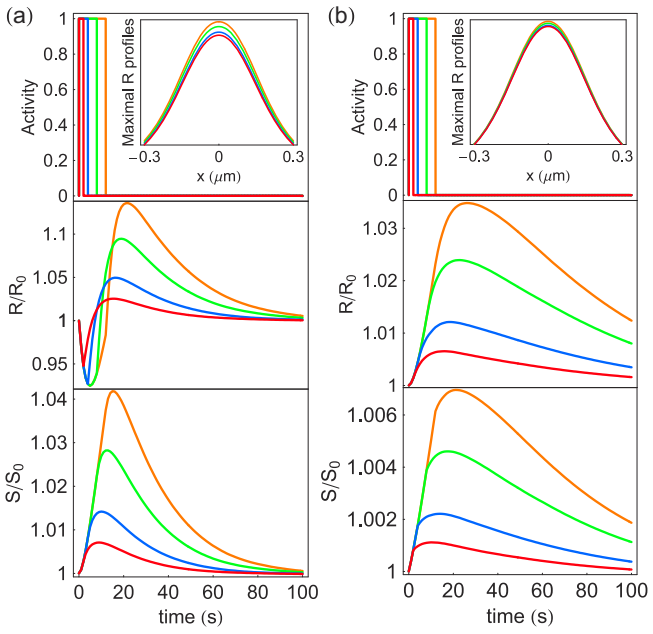

FIG. 5: (Color online) Short-term plasticity of synaptic receptor domains induced by spatiotemporal modulations of the diffusion rate. Response of an individual RSD to synaptic stimulation implemented as (a) a local increase in the receptor diffusion rate or (b) a local decrease in the scaffold diffusion rate. Top panels: duration of step stimulations. Insets: receptor concentration profiles at times of maximum domain size. Middle (bottom) panels: time course of the total in-domain receptor (scaffold) population size, R (S), following stimulation, normalized by the total in-domain receptor (scaffold) population size in the absence of any stimulation, R_0 (S_0). The results in panel (a) (panel (b)) were obtained by simulating Eqs. (1) and (2) with $D_s(x,y,t) = 1$ ($D_r(x,y,t) = 1$) and a locally increased $D_r(x,y,t) > 1$ (a locally decreased $D_s(x,y,t) < 1$), using the reaction kinetics of model C in Table I. The duration of stimulation in panels (a) and (b) was 2 s, 4 s, 8 s, and 12 s, and the stimulation strength (fractional increase or decrease in receptor or scaffold diffusion rate) was identical for panels (a) and (b), and ten times stronger than in Fig. 4(c). Reaction and diffusion rates were chosen as specified in Eq. (C8). (See Appendix C for further details; top and middle panels of (a) as in Ref. [29] and shown here for completeness.)

We implemented [29] synaptic activity in our reaction-diffusion model of synaptic receptor domains through a local increase (Fig. 5(a)), or a local decrease (Fig. 5(b)), in the receptor, or scaffold, diffusion rate, respectively. As shown in Fig. 5, with this representation of synaptic activity we found, once the pre- and postsynaptic parts of the synapse were aligned, a transient increase in the synaptic receptor population due to synaptic activity. A notable feature of both scenarios in Fig. 5 is that the increase in the receptor population extended for a longer time than the synaptic activity. Furthermore, while the receptor and scaffold concentrations both increased, the size of the RSDs remained approximately constant. We also observed that if receptor and scaffold diffusion rates were increased or decreased together by an equal fraction, there entailed little change in the in-domain receptor and scaffold populations.

The behavior described above follows from the interplay between the inhibitors (receptors) and activators (scaffolds) in our reaction-diffusion model. Once synaptic activity is turned on, membrane regions with an increased receptor diffusion rate (a decreased scaffold diffusion rate) are initially distinguished by a relative decrease in the receptor population (increase in the scaffold population) because the net diffusion current of receptors (scaffolds) out of postsynaptic membrane domains is increased (decreased). However, since the receptors are the inhibitors, and the scaffolds the activators, of increased molecular concentrations in our reaction-diffusion model, more receptors as well as more scaffolds are drawn into such regions through the receptor and scaffold reaction kinetics, leading to a shift in the dynamic steady state responsible for the spontaneous formation of stable RSDs (Fig. 1(b)) and an increased receptor population. A notable qualitative difference between the evolution of the receptor populations in Figs. 5(a) and 5(b) is that, in the case of synaptic activity implemented as a local increase in the receptor diffusion rate, the prolonged increase in receptor concentration is preceded by a brief, transient decrease in receptor population. Again, this behavior follows from the temporary increase in the net receptor diffusion current out of postsynaptic membrane domains in Fig. 5(a), together with the coupling of receptor and scaffold reaction kinetics. Finally, Fig. 5 shows that, for a given fractional change in receptor or scaffold diffusion rate, a local increase in the receptor diffusion rate produces a greater increase in receptor population.

V. DISCUSSION

A. Summary and outlook

Based on previous experimental and theoretical work [29], we have developed a reaction-diffusion (Turing) model which describes the spontaneous self-assembly of stable postsynaptic receptor domains. The proposed reaction-diffusion model explains how a small set of interactions between receptors and scaffolds is sufficient for the formation of stable postsynaptic receptor domains of the characteristic size observed in neurons and transfected non-neural cells [26, 27, 29, 38], and why no presynaptic or otherwise sophisticated molecular machinery may be necessary for the emergence of postsynaptic receptor domains. Using reaction and diffusion rates within the broad ranges of values suggested by experiments, the spatial scales and geometry of the simulated arrays of domains, as well as the time scale of their emergence, are consistent with experimental observations.

At the heart of the model is a linear (Turing) instability, for which the differential diffusion of receptor and scaffold molecules is essential and which triggers the for-

mation of synaptic domains. This same mechanism can also explain a preferential alignment of pre- and postsynaptic molecular machineries (provided that presynaptic activity alters the diffusive properties of receptor or scaffold molecules) and, further, suggests a new form of short-term postsynaptic plasticity [5–7]. In particular, our model predicts that the receptor and scaffold populations in RSDs can be increased through a local increase in the receptor diffusion rate or a local decrease in the scaffold diffusion rate. For instance, our simulations indicate that an increase (decrease) in the receptor (scaffold) diffusion coefficient by 20% can enhance the total receptor population in RSDs by more than 10% (3%) (Fig. 5). Experimental observations indeed suggest [3, 7, 48–55] that synaptic activity may modify receptor or scaffold diffusion. Quantitative measurements of the magnitude and sign of activity-induced changes in receptor or scaffold diffusion, and the resulting changes in synaptic receptor populations, may allow direct experimental tests of the speculative mechanism for short-term postsynaptic plasticity suggested by our reaction-diffusion model.

Following Turing's seminal theoretical and computational work [39, 64] on the spontaneous formation of stable biological patterns with a well-defined characteristic wavelength [40–47] from random initial conditions, concerted experimental and theoretical efforts to align reaction-diffusion models more closely with pattern formation in specific biological systems have begun to bear fruit over recent years [60, 61]. In particular, reaction-diffusion models have been invoked in the context of morphogenesis in multicellular organisms [65–68] to address how, in the absence of any pre-existing pattern [61, 69], cells can be endowed with positional information. More recently, reaction-diffusion models have been employed [70–77] to understand how cells determine the cell center as the site of cell division. Here, we use similar concepts to describe the self-assembly of stable RSDs. RSD formation, unlike morphogenesis and spatial cell regulation, occurs on a subcellular scale: domains are localized at different locations on the cell membrane and do not extend over the whole cell membrane.

The model developed here provides a conceptual bridge that connects the 'mesoscopic' realm of synaptic receptor domains to the 'microscopic' realm of synaptic receptor and scaffold molecules; the former, in order to carry out a biological function, must be stable over long times scales, while the latter is governed by rapid chemical reactions and diffusion processes. Our model constitutes a step towards the goal [9, 10, 30] of unraveling the minimal molecular components required for the maturation, maintenance, and regulation of synapses. Alongside other recent applications of reaction-diffusion models that aim at uncovering the molecular mechanisms responsible for biological pattern formation [60, 61], the model we discussed here, together with potential new experiments it can help design, may bring us closer to a quantitative understanding of the relations between the properties of biologically important supramolecular structures and the dynamics and interactions that rule their components.

B. Relation of model predictions and experimental observations

A number of experimental studies [9, 10, 29–36], carried out on a variety of synapses, suggest that domains of synaptic receptor molecules form spontaneously even in the absence of presynaptic terminals. In particular, in our minimal model system [29] the presence of glycine receptors and gephyrin scaffolds is sufficient for the formation of synaptic receptor domains of the stable characteristic size reported [14, 26, 37] for neurons and transfected non-neural cells. The reaction-diffusion model of synaptic receptor domains provides a quantitative explanation for the spontaneous formation of RSDs of a stable characteristic size. Indeed, our model predicts that the characteristic size of RSDs is set by the reaction and diffusion properties of receptors and scaffolds (see Eq. (23)).

A crucial feature of the proposed reaction-diffusion model is that the formation of membrane domains composed of receptors or scaffolds can only occur if receptors and scaffolds are both present (Fig. 1(b)), which is in agreement with experimental observations [26, 27, 38] on cells transfected with only glycine receptors or gephyrin scaffolds. Our simulations show that the characteristic scale and time of formation of the patterns produced by our reaction-diffusion model are consistent with the experimental patterns of RSDs [14, 26, 29]. In particular, irregular patterns of RSDs emerge over a time scale of hours, and ultimately individual RSDs occupy an area of approximately 0.2 to 0.3 μm^2. The resulting profiles of receptor and scaffold concentrations are in phase and the cluster shapes and positions are stable. The reaction-diffusion model of synaptic receptor domains predicts [29] that the receptor and scaffold concentration profiles are inhomogeneous across RSDs, with a maximal concentration of receptors and scaffolds at the center of RSDs, and that the receptor concentration profiles across RSDs are broader than the scaffold concentration profiles.

One mathematical constraint imposed by the model is of particular note: in our model, a crucial reaction for the formation of synaptic receptor domains is the stabilization of a scaffold molecule at the membrane by two other scaffold molecules already present at the membrane (see Table I). Gephyrin scaffold molecules are indeed thought to form both dimers and trimers on the neural membrane, in the natural conditions in which synaptic receptor domains are observed [9]. However, if trimerization of gephyrin molecules is prevented, no glycine receptor domains (or only very small ones) appear [14], in agreement [29] with our reaction-diffusion model. Similarly, the reaction-diffusion model of synaptic receptor domains predicts that no stable domains of receptors and scaffolds appear if stabilizing receptor-scaffold interactions, such as the (transient) binding of glycine receptors by gephyrin scaffolds at the membrane, are disabled.

Moreover, our model predicts that receptor aggregation trails behind [29] scaffold aggregation in time during receptor domain formation (Fig. 1(b)). This indeed appears to be in agreement with experimental observations [78, 79]. The corollary to this model prediction—namely, that a loss of scaffolds precedes a decrease in the receptor population—is also consistent with recent *in vivo* experiments [80].

While we find that the gross features of synaptic receptor domains obtained from our mathematical model and observed in the corresponding minimal experimental system [29] are in agreement with synaptic receptor domains in neurons, a quantitative description of the self-assembly and plasticity of synaptic receptor domains in neurons will necessitate consideration of the full complexity of the synaptic apparatus [2, 4, 8, 10]. In particular, mature synapses involve interactions between thousands of proteins, interactions between pre- and postsynaptic domains, and, possibly, an interplay between membrane geometry and the formation and dynamics of synaptic receptor domains. Such additional layers of complexity do not, in principle, invalidate the reaction-diffusion mechanism for pattern formation discussed here, which has been successfully employed to understand the spontaneous emergence of ordered molecule distributions in a variety of highly complex biological systems [45–47, 60, 61, 70–77] (see Appendix D for a discussion of possible model extensions and modifications).

C. Open questions

In our model, molecular domains emerge from the combined presence of 'activator' scaffold molecules, which bind themselves as well as receptors, and receptors, which act as 'inhibitors' due to their steric repulsion. Would the converse scheme, in which scaffolds play the role of inhibitors and receptors play the role of activators, provide an alternate candidate model? Experimental results [1–4, 9–14] and quantitative reasoning suggest arguments both ways.

The observation that receptors are less numerous than scaffolds in domains, by about an order of magnitude [8], suggests that steric repulsion may be more significant for scaffolds than for receptors (and, indeed, we also included steric repulsion between scaffolds in our model). Furthermore, the fact that bound receptor-scaffold complexes can be ferried from the cytoplasm to the membrane suggests that receptors may act as activators by tending to 'pin' scaffolds at the membrane; indeed, receptors can spend an appreciable time at the membrane in the absence of scaffolds, while the reverse may not be true. These remarks tend to a picture in which receptors play the role of activators and scaffolds that of inhibitors, at odds with our model. However, scaffolds are known to be autocatalytic, as required for 'activators', and domains disappear if their trimerization is prevented. By contrast, as putative 'activators' receptors would have to be autocatalytic via indirect reactions, and it is not obvious that these would yield a Turing instability. Finally, one would need $\nu_s > \nu_r$ if receptors were to play the role of activators, which is not validated by experiments.

Yet, it may be possible to devise an alternate model, in which receptors stabilize scaffolds, rather than the reverse, and which is also consistent with the basic experimental phenomenology of RSDs; we relegate the investigation of such a 'converse model' to a later study. We note, however, that a model which goes some length in this direction is discussed in Ref. [22]. There, domain evolution is not governed by a reaction-diffusion mechanism, but rather by a convection-aggregation mechanism. It bares some similarities to models of phase separation through diffusion and clustering [81, 82], in which, generically, domains continue to coarsen and have no stable characteristic size. Thus, the respective roles of the different molecular species and the stability of domains in such models may have to be considered with some care.

Some aspects of our model will have to be explored in greater detail or extended. While we find, indeed, that the time scale of emergence and stabilization of synaptic domains corresponds to the experimental time scale, this result is surprising in that these very long time scales emerge from relatively simple reaction-diffusion equations that contain only short time scales. One would like to gain a more thorough understanding of the way in which collective long time scales emerge in the patterning process. Furthermore, the reaction and diffusion rates used in our simulations are difficult to measure directly and, for the most part, only broad ranges for these parameters are available from experiments. Indeed, experiments address quantities such as the turnover of receptors on the membrane; the time scale associated with the latter may reflect the concatenation of a large number of chemical reactions. By contrast, in the reaction-diffusion model of synaptic receptor domains 'bare' rates are used, which correspond to individual chemical reactions. New experiments will be necessary to extract microscopic time scales and, possibly, new theory will be required to relate these to the effective time scales currently measured in experiments. Similarly, while the diffusion properties of synaptic receptors, such as the glycine receptors considered here, have been experimentally characterized in some detail [3, 9–11, 14, 27], the corresponding data on scaffold diffusion, which is needed for a quantitative description of RSDs, is less complete.

Finally, throughout we have focused on a mean-field description of RSDs, and we ignored the molecular noise induced by the underlying reaction and diffusion processes. As described in Appendix A, noise can be incorporated systematically into our reaction-diffusion model and, indeed, the low copy number of receptors and scaffolds in RSDs suggests [8] that noise may play an important role in the formation and stability of RSDs. Previous theoretical work [83, 84] has shown that molecular noise can have intriguing effects on reaction-diffusion patterns, and even stabilize the self-assembly of reaction-diffusion

domains against perturbations in the reaction or diffusion rates. Thus, complementary to the rapid molecular turnover we focused on here, molecular noise may also help to stabilize RSDs against molecular perturbations.

Acknowledgments

R.A.d.S. is grateful to Vincent Hakim for thought-provoking conversations. This work was supported by an Alfred P. Sloan Research Fellowship in Physics and NSF Award DMR-1206332 (CAH), NSF Award DMR-1206323 (MK), Inserm UR 789 (AT), and UMR 8550 (RAdS).

Appendix A: Lattice model of receptor and scaffold reaction and diffusion dynamics

Following similar steps as in previous work on lattice models in population biology [56–58], we derive Eqs. (1) and (2) from a lattice model of reaction and diffusion dynamics. In this model, the system is discretized so that reactions only occur between molecules which simultaneously occupy a lattice site (membrane patch) (i,j), while receptor and scaffold molecules are allowed to hop randomly from one lattice site to a nearest-neighbor site. We denote the hopping rates of receptors and scaffolds at site (i,j) by $D^{(R)}_{i,j}/\tau_R$ and $D^{(S)}_{i,j}/\tau_S$, respectively. Reaction and diffusion processes are only permitted if the resultant lattice configuration satisfies the condition $0 \leq R_{i,j} + S_{i,j} \leq 1$ at all lattice sites, where $R_{i,j}/\epsilon$ and $S_{i,j}/\epsilon$ denote the occupation numbers of receptor and scaffold molecules at site (i,j), and we have introduced the normalization constant ϵ so that the maximum particle number per lattice site is equal to $1/\epsilon$. A more complicated crowding condition, $0 \leq AR_{i,j} + BS_{i,j} \leq 1$, in which receptors and scaffolds are weighed differently according to two constants A and B, would be possible, too, but would raise the number of parameters in the model. For the sake of simplicity, we set $A = B = 1$. For the sake of simplicity, also, we consider a square lattice, but all considerations are readily extended to other lattice symmetries.

The lattice model described above is Markovian and, hence, completely characterized by the occupation numbers $\mathbf{R}(t) = (R_{1,1}(t), R_{1,2}(t), \ldots, R_{L,L}(t))$ and $\mathbf{S}(t) = (S_{1,1}(t), S_{1,2}(t), \ldots, S_{L,L}(t))$ at time t for a lattice of size $L \times L$. The dynamics of the model are governed by a set of coupled master equations [85] for the probabilities that the configurations are $\mathbf{R}$ and $\mathbf{S}$ at time t. The central quantities in this formulation are $W_N(\mathbf{N};\mathbf{m})$, the transition rates for switching from a configuration $\mathbf{N}$ to a configuration $\mathbf{N}+\mathbf{m}$, where $\mathbf{N} = \mathbf{R}$ or $\mathbf{N} = \mathbf{S}$. Following the approach developed in Refs. [85–88], we transform these master equations into the more tractable lattice Langevin equations

$$\frac{dR_{i,j}}{dt} = K^{(R;1)}_{i,j} + \eta^{(R)}_{i,j}\,, \tag{A1}$$

$$\frac{dS_{i,j}}{dt} = K^{(S;1)}_{i,j} + \eta^{(S)}_{i,j}\,, \tag{A2}$$

where $K^{(R,S;1)}_{i,j}$ are the first moments of the transition rates W_R and W_S, and the $\eta^{(R,S)}_{i,j}$ are Gaussian noises that have zero mean and covariance

$$\langle \eta^{(N)}_{i,j}(t_1)\, \eta^{(N)}_{k,l}(t_2)\rangle = K^{(N;2)}_{i,j;k,l}\, \delta(t_1 - t_2)\,, \tag{A3}$$

for $N = R$ or $N = S$, where $K^{(N;2)}_{i,j;k,l}$ are the second moments of the transition rates, and $\delta(x)$ is the Dirac-delta function. The transition moments are defined as

$$K^{(N;1)}_{i,j}(\mathbf{N}) = \int m_{i,j}\, W_N\,(\mathbf{N};\mathbf{m})\; d\mathbf{m}\,, \tag{A4}$$

$$K^{(N;2)}_{i,j;k,l}(\mathbf{N}) = \int m_{i,j}\, m_{k,l}\, W_N\,(\mathbf{N};\mathbf{m})\; d\mathbf{m}\,. \tag{A5}$$

On a formal level, Eqs. (A1) and (A2), together with Eqs. (A3)–(A5), completely specify our lattice model.

The rules of our lattice model enter the Langevin equations (A1) and (A2) through the expressions for W_R and W_S. Each of these transition rates is a sum of contributions due to diffusion and reactions. The transition rates for the diffusion processes take the form

$$W_d = W^{(1)}_d + W^{(2)}_d + W^{(3)}_d + W^{(4)}_d\,, \tag{A6}$$

in which $W^{(k)}_d$, with $k = 1, 2, 3$, or 4, denote the transition rates for hopping from site (i,j) to the sites $(i \pm 1, j \pm 1)$. We have

$$W^{(k)}_d\,(\mathbf{N};\mathbf{m}) = \frac{1}{4\tau_N} \sum_{i,j} \mathcal{E}^{(k)}_{i,j} D^{(N)}_{i,j} \delta\,(m_{i,j} + \epsilon)\; \delta\,(m_{i\pm1,j\pm1} - \epsilon) \prod_{(p,q)\neq(i,j),(i\pm1,j\pm1)} \delta\,(m_{p,q})\;, \tag{A7}$$

where the summation extends over all lattice sites and the exclusion condition $\mathcal{E}^{(k)}_{i,j}$ is

$$\mathcal{E}^{(k)}_{i,j} = N_{i,j}\; [1 - (R_{i\pm1,j\pm1} + S_{i\pm1,j\pm1})]\;, \tag{A8}$$

and $N_{i,j} = R_{i,j}$ or $N_{i,j} = S_{i,j}$. Substituting Eq. (A7) into Eq. (A6) and using Eq. (A4), we calculate the first moment

of the hopping rates of receptors or scaffolds constrained by the bounds $0 \leq R_{i,j} + S_{i,j} \leq 1$ as

$$\begin{aligned} K_{i,j}^{(d;1)} = & -\frac{\epsilon}{4\tau_N}\Big(D_{i,j}^{(N)} N_{i,j}\left[1-(R_{i+1,j}+S_{i+1,j})\right] + D_{i,j}^{(N)} N_{i,j}\left[1-(R_{i-1,j}+S_{i-1,j})\right] \\ & + D_{i,j}^{(N)} N_{i,j}\left[1-(R_{i,j-1}+S_{i,j-1})\right] + D_{i,j}^{(N)} N_{i,j}\left[1-(R_{i,j+1}+S_{i,j+1})\right]\Big) \\ & + \frac{\epsilon}{4\tau_N}\left(D_{i+1,j}^{(N)} N_{i+1,j} + D_{i-1,j}^{(N)} N_{i-1,j} + D_{i,j-1}^{(N)} N_{i,j-1} + D_{i,j+1}^{(N)} N_{i,j+1}\right)\left[1-(R_{i,j}+S_{i,j})\right] \end{aligned} \tag{A9}$$

for $N_{i,j} = R_{i,j}$ or $N_{i,j} = S_{i,j}$. The above expression provides a direct microscopic interpretation of the nonlinear diffusion terms in Eqs. (1) and (2): The first (negative) term in Eq. (A9) arises from the random hopping of particles away from site (i, j), whereas the second (positive) term corresponds to transitions onto site (i, j). Also note from Eq. (A9) that our formulation of diffusion conserves the particle number, and that the number of receptors or scaffolds per lattice site cannot decrease below zero or increase beyond $1/\epsilon$. Rearranging Eq. (A9) we find

$$K_{i,j}^{(R,d;1)} = \frac{\epsilon}{4\tau_R}\left[(1-R_{i,j}-S_{i,j})\,\Delta^2\left(D_{i,j}^{(R)} R_{i,j}\right) + D_{i,j}^{(R)} R_{i,j}\left(\Delta^2 R_{i,j} + \Delta^2 S_{i,j}\right)\right], \tag{A10}$$

$$K_{i,j}^{(S,d;1)} = \frac{\epsilon}{4\tau_S}\left[(1-R_{i,j}-S_{i,j})\,\Delta^2\left(D_{i,j}^{(S)} S_{i,j}\right) + D_{i,j}^{(S)} S_{i,j}\left(\Delta^2 R_{i,j} + \Delta^2 S_{i,j}\right)\right], \tag{A11}$$

in which the discrete second derivative operator

$$\Delta^2 N_{i,j} = N_{i-1,j} + N_{i,j-1} - 4N_{i,j} + N_{i+1,j} + N_{i,j+1} \tag{A12}$$

acts on all indices (i, j) in Eqs. (A10) and (A11). For a single particle species with a constant diffusion rate the above expressions would simply reduce to a discrete Laplacian operator with square symmetry acting on $R_{i,j}$ or $S_{i,j}$. This is of course to be expected for unbiased random hopping. (With a bias in the hopping rates one would obtain a discrete version of the Burgers equation [89].) Expressions of the second moments for random hopping with thresholds $0 \leq R_{i,j} + S_{i,j} \leq 1$, which capture the effects of diffusive noise in Eqs. (A1) and (A2), can be obtained by following similar steps as above. As an alternative to the continuum approach we focus on in this article, particle-based approaches [90, 91] could be used to quantify steric effects on the diffusion of individual receptors and scaffolds.

The transition rates for the chemical reactions in our reaction-diffusion model take the generic form

$$W_c(\mathbf{N};\mathbf{m}) = \sum_{i,j} \mathcal{R}_{i,j}\,\delta(m_{i,j} \pm \epsilon) \prod_{(k,l)\neq(i,j)} \delta(m_{k,l}), \tag{A13}$$

in which $\mathcal{R}_{i,j}$ incorporates the details of the specific reaction under consideration. For instance, for the reaction $R_b + R + S \longrightarrow 2R + S$ we have

$$\mathcal{R}_{i,j} = \alpha_1[1-(R_{i,j}+S_{i,j})]R_{i,j}S_{i,j}, \tag{A14}$$

where α_1 is the reaction rate associated with $R_b + R + S \longrightarrow 2R + S$, with analogous expressions for all other reactions in Table I [92, 93]. From Eqs. (A4) and (A5), the first and second moments associated with Eq. (A13) are

$$K_{i,j}^{(N,c;1)} = \pm\epsilon\mathcal{R}_{i,j}, \tag{A15}$$

$$K_{i,j}^{(N,c;2)} = \epsilon^2\mathcal{R}_{i,j}, \tag{A16}$$

which determine the parts of the lattice Langevin equations (A1) and (A2) describing the reactions in our reaction-diffusion model.

Using the above expressions of the transition moments associated with diffusion and reaction processes, we obtain simplified versions of the lattice Langevin equations (A1) and (A2) by introducing the continuous fields $r(x, y, t)$, $s(x, y, t)$, and $D_{r,s}(x, y, t)$:

$$F(i\pm n, j\pm m, t) = \sum_{k,l=0}^{\infty}\left(\frac{\partial^{k+l} f}{\partial x^k \partial y^l}\right)\Big|_{(i,j)} \frac{(\pm a\,n)^k}{k!}\,\frac{(\pm a\,m)^l}{l!}, \tag{A17}$$

for $F = R,\ S,\ D^{(R,S)}$ and $f = r,\ s,\ D_{r,s}$, respectively, where a is the lateral lattice spacing. Employing Eq. (A17) and setting $\nu_{r,s} = \epsilon a^2/4\tau_{R,S}$, the deterministic parts of Eqs. (A1) and (A2) are, to lowest order, equivalent to the reaction-diffusion model in Eqs. (1) and (2). The continuum limit of the first moment of the reaction processes in Eq. (A15) thereby yields [92, 93] terms consistent with the standard formalism of chemical dynamics [40–47], while the first moments of receptor and scaffold diffusion yield the generalized diffusion currents in Eqs. (3) and (4). In particular, in agreement with previous studies of similar lattice models [56–58] we find that, if receptors and scaffolds are both present, steric repulsion between receptors and scaffolds yields non-linear contributions to the mean-field diffusion currents as in Eqs. (3) and (4).

Appendix B: Reaction kinetics for receptor-scaffold aggregation

In this appendix we provide a detailed discussion of how the mathematical conditions in Eqs. (17)–(19), together with the basic experimental phenomenology of interactions between glycine receptors and gephyrin scaf-

folds [3, 8–11], motivate the reaction schemes in Table I. First, consider the polynomial $F = F(r,s)$ in Eq. (1). The lowest-order reaction in which receptors are activated by scaffolds is the first-order reaction $R_b + S \longrightarrow R + S$. For $(r,s) = (\bar{r},\bar{s})$ to be a nontrivial fixed point, this 'activation' (adsorption at the membrane) of r must be compensated by 'inhibition' (desorption from the membrane) [40–47]. The lowest-order reaction which decreases r while respecting $0 \leq r \leq 1$ is $R \longrightarrow R_b$. Thus, the most basic expression of F is given by

$$F(r,s) = \underbrace{b\frac{\bar{r}}{\bar{s}}Es}_{R_b+S\longrightarrow R+S} \underbrace{-br}_{R\longrightarrow R_b} , \tag{B1}$$

which is equivalent to the receptor reaction kinetics for model A in Eq. (13). (Recall that $E = (1-r-s)/(1-\bar{r}-\bar{s})$.) Below each term in Eq. (B1) we have indicated the corresponding chemical reaction. Equation (B1) is easily extended to include additional reactions.

To determine $G = G(r,s)$ we assume that receptor molecules do not actively remove scaffold molecules from the cell membrane, but passively inhibit s through steric constraints. The lowest-order reaction through which s activates its own production is $S_b + S \longrightarrow 2S$. To ensure that $(r,s) = (\bar{r},\bar{s})$ is indeed a non-trivial fixed point, this reaction must be balanced by a reaction depleting s. However, it is not possible to choose this reaction at first (or second) order such that the conditions $0 \leq s \leq 1$ and $s_{22} > 0$ are both satisfied, where the latter condition mandates that, consistent with the basic phenomenology of gephyrin [3, 9–11], scaffolds stabilize other scaffolds around the homogeneous fixed point $(r,s) = (\bar{r},\bar{s})$. At second order, there are two possible reactions that activate s: $S_b + S + R \longrightarrow 2S + R$ and $S_b + 2S \longrightarrow 3S$. For the first of these reactions, one again finds upon expanding $G(r,s)$ that this reaction cannot be balanced by a reaction depleting s at first or second order such that $0 \leq s \leq 1$ and $s_{22} > 0$.

But the reaction $S_b + 2S \longrightarrow 3S$ can activate s while satisfying Eqs. (17)–(19). The lowest-order inhibiting processes associated with $S_b + 2S \longrightarrow 3S$ are $S \longrightarrow S_b$ and $M_b + S \longrightarrow S_b + M_b$, respectively. The expression of G obtained with the first of these inhibiting reactions is

$$G(r,s) = \underbrace{-\mu s}_{S\longrightarrow S_b} \underbrace{+\frac{\mu}{\bar{s}}Es^2}_{S_b+2S\longrightarrow 3S} , \tag{B2}$$

which can satisfy $s_{22} > 0$ as well as $s_{21} < 0$ so that scaffolds are inhibited by receptors (but see the discussion in Sec. IV A). The reaction $M_b + S \longrightarrow S_b + M_b$, however, yields $s_{21} > 0$ if the steric constraint affects a temporary adsorption of species M_b at the membrane. But one can clearly include additional reactions which ensure that $s_{21} < 0$. To low order, this is achieved by including (transient) dimerization of scaffolds [3, 9], which extends the reaction kinetics to

$$G(r,s) = \underbrace{-\beta s}_{S\longrightarrow S_b} \underbrace{+(\beta-\mu)\,Es}_{S_b+S\longrightarrow 2S} \underbrace{+\frac{\mu}{\bar{s}}Es^2}_{S_b+2S\longrightarrow 3S} , \tag{B3}$$

where we have assumed that $\beta > \mu$. Equation (B3) is equivalent to the expression of G for model A in Eq. (14).

Model B in Table I is obtained by combining the receptor reaction kinetics in Eq. (B1) with the scaffold reaction kinetics in Eq. (B2):

$$F_B(r,s) \equiv F_A(r,s) , \tag{B4}$$

$$G_B(r,s) = \mu\frac{s}{\bar{s}}\,(Es - \bar{s}) . \tag{B5}$$

We note that scaffold molecules must necessarily be activated by a second-order reaction while F in Eq. (B1) only involves reactions up to first order, which motivates the inclusion of reactions of the same order in F as in G, and *vice versa*. For model A this yields model A′ in Table I,

$$F_{A'}(r,s) = -b\left(r - \frac{s}{\bar{s}}E\bar{r}\right) + m\frac{s}{\bar{s}}E\,(r-\bar{r}) , \tag{B6}$$

$$G_{A'}(r,s) = G_A(r,s) , \tag{B7}$$

where m is a constant, while for model B we obtain model B′ in Table I,

$$F_{B'}(r,s) = -b\left(r - \frac{s}{\bar{s}}E\bar{r}\right) + m\frac{r}{\bar{r}}\,(Es - \bar{s}) , \tag{B8}$$

$$G_{B'}(r,s) = -\beta\,(s - E\bar{s}) + \mu\frac{s}{\bar{s}}\,(Es - \bar{s}) . \tag{B9}$$

Finally, combining the various reactions included in models A, A′, B, and B′, we arrive at model C in Table I:

$$F_C(r,s) = \underbrace{-br}_{R\longrightarrow R_b} \underbrace{+m_1E\bar{r}}_{R_b\longrightarrow R} \underbrace{-\left(m_1 + m_2\frac{\bar{s}}{\bar{r}}\right)Er}_{M_b+R\longrightarrow M_b+R_b} \underbrace{+bE\frac{\bar{r}}{\bar{s}}s}_{R_b+S\longrightarrow R+S} \underbrace{+\frac{m_2}{\bar{r}}Ers}_{R_b+R+S\longrightarrow 2R+S} , \tag{B10}$$

$$G_C(r,s) = \underbrace{-\beta s}_{S\longrightarrow S_b} \underbrace{+\beta E\,\bar{s}}_{S_b\longrightarrow S} \underbrace{-\mu Es}_{M_b+S\longrightarrow S_b+M_b} \underbrace{+\frac{\mu}{\bar{s}}Es^2}_{S_b+2S\longrightarrow 3S} , \tag{B11}$$

where m_1 and m_2 are constants. From a biological perspective it is particularly noteworthy that model C includes endocytosis and insertion of receptor and scaffold molecules as well as the reactions $M_b + R \longrightarrow R_b + M_b$ and $M_b + S \longrightarrow S_b + M_b$, which correspond to the removal of receptor and scaffold molecules from the cell membrane by a bulk molecule M_b or by some alternate molecular mechanism which involves a temporary increase in the local crowding of the cell membrane.

We note that model C does not encompass all reactions up to some specified order. Rather, we constructed model

C by including all reactions suggested by experimental observations [3, 9–11]. Model C could be supplemented, for instance, by reactions such as $S_b + S + R \longrightarrow 2S + R$. In all our formulations of the reaction kinetics in Table I, several reactions could be freely added without actually changing the model. For example, in model C we consider the reaction $M_b + R \longrightarrow R_b + M_b$ in F. The reaction $R_b + R \longrightarrow 2R$ is then automatically included because of the identity

$$-Er\left[\alpha_2(1-\bar{r}-\bar{s})\right] + \alpha_2(1-r-s)r \equiv 0\,, \qquad \text{(B12)}$$

where α_2 is the reaction rate associated with the reaction $R_b + R \longrightarrow 2R$. Note, however, that α_2 is necessarily smaller here than the overall reaction rate of $M_b + R \longrightarrow R_b + M_b$.

Appendix C: Simulation of reaction-diffusion equations

To simulate a given model of the reaction-diffusion dynamics, we solved numerically the dimensionless versions of Eqs. (1) and (2) using the variables

$$x \to \widetilde{x} = \sqrt{\frac{b}{\nu_r}}\,x\,,\ y \to \widetilde{y} = \sqrt{\frac{b}{\nu_r}}\,y\,,\ t \to \widetilde{t} = b\,t\,, \quad \text{(C1)}$$

in terms of which Eqs. (1) and (2) become

$$\frac{\partial r}{\partial \widetilde{t}} = \widetilde{F} + \widetilde{\nabla}\left[D_r(1-s)\widetilde{\nabla}r + D_r r\widetilde{\nabla}s + \overline{E}r\widetilde{\nabla}D_r\right]\,, \qquad \text{(C2)}$$

$$\frac{\partial s}{\partial \widetilde{t}} = \widetilde{G} + \widetilde{\nu}_s\widetilde{\nabla}\left[D_s(1-r)\widetilde{\nabla}s + D_s s\widetilde{\nabla}r + \overline{E}s\widetilde{\nabla}D_s\right]\,, \qquad \text{(C3)}$$

where $\overline{E} = 1 - r - s$, $\widetilde{F} = \widetilde{F}\,(r, s; \widetilde{m})$ or, depending on the model formulation considered, $\widetilde{F} = \widetilde{F}\,(r, s; \widetilde{m_1}, \widetilde{m_2})$, $\widetilde{G}(r,s) = \widetilde{G}\left(r, s; \widetilde{\beta}, \widetilde{\mu}\right)$, and

$$\left(\widetilde{m}, \widetilde{m_1}, \widetilde{m_2}, \widetilde{\beta}, \widetilde{\mu}\right) = \frac{1}{b}\,(m, m_1, m_2, \beta, \mu)\ , \quad \text{(C4)}$$

$$\widetilde{\nu_s} = \frac{\nu_s}{\nu_r}\,, \quad \widetilde{\nabla} = \left(\frac{\partial}{\partial\widetilde{x}}, \frac{\partial}{\partial\widetilde{y}}\right)\,. \qquad \text{(C5)}$$

Physical dimensions were restored to the solutions of Eqs. (C2) and (C3) using representative values of ν_r and b measured in experiments. In particular, experiments on the diffusion of glycine receptors [3, 9–11, 14, 27] suggest $\nu_r = 10^{-2}\ \mu\text{m}^2\ \text{s}^{-1}$ as a typical value of the receptor diffusion coefficient, although measurements of ν_r are complicated by interactions between receptors and scaffolds, as well as crowding in the cell membrane. We used $\nu_r = 10^{-2}\ \mu\text{m}^2\ \text{s}^{-1}$ for all the calculations described here. For the rate of receptor turnover, experiments have indicated [3, 9, 10] characteristic time scales ranging from seconds to hours. These time scales, assuming they are related directly to the rates entering our model, yield values of b ranging from $b = 10^{-1}\ \text{s}^{-1}$, which we used for Figs. 2, 3(a), 4, and 5, to $b = 10^{-4}\ \text{s}^{-1}$, which we used for Figs. 3(b) and 3(c).

TABLE II: Approximate receptor reaction rates in Eq. (1) for various reaction schemes. All rates were estimated to one significant figure from Eqs. (C6)–(C9) and are quoted in units of s^{-1}.

Contributions to F	Model A	Model B′	Model C
$R \longrightarrow R_b$	1×10^{-1}	8×10^{-1}	1×10^{-1}
$R_b \longrightarrow R$	0	0	$2 \times 10^{-3}\,\overline{E}$
$M_b + R \longrightarrow R_b + M_b$	0	0	$1\,\overline{E}$
$R_b + S \longrightarrow R + S$	$1 \times 10^{-1}\,\overline{E}$	$1 \times 10^{-1}\,\overline{E}$	$1 \times 10^{-1}\,\overline{E}$
$R_b + R + S \longrightarrow 2R + S$	0	$2 \times 10\,\overline{E}$	$2 \times 10\,\overline{E}$

Various experiments have indicated [3, 9–11, 13, 14, 27] that $\nu_s \ll \nu_r$ for synaptic receptors and scaffolds and, hence, $\widetilde{\nu}_s \ll 1$. In our simulations we used values of $\widetilde{\nu}_s$ in the range $(0.01, 0.05)$. In the absence of precise, quantitative measurements of ν_s, we chose phenomenological values $\widetilde{\nu}_s \ll 1$ which satisfied the mathematical constraint in Eq. (19) for a given formulation of the reaction kinetics. Similarly, we used values of the dimensionless reaction rates consistent with Eqs. (17) and (18), and the available experimental data on receptor and scaffold reaction kinetics [3, 9–11]. The patterns in Fig. 2 were obtained using the (dimensionless) parameter values

$$(\widetilde{\beta}, \widetilde{\mu}, \widetilde{\nu}_s) = (7, 0.7, 0.05)\,, \qquad \text{(C6)}$$

$$(\widetilde{m}, \widetilde{\beta}, \widetilde{\mu}, \widetilde{\nu}_s) = (7, 0.7, 1.2, 0.05)\,, \qquad \text{(C7)}$$

$$(\widetilde{m}_1, \widetilde{m}_2, \widetilde{\beta}, \widetilde{\mu}, \widetilde{\nu}_s) = (0.4, 10, 0.5, 0.7, 0.02) \qquad \text{(C8)}$$

for panels (a), (b), and (c), respectively. The results in Fig. 3 were obtained with

$$(\widetilde{\beta}, \widetilde{\mu}, \widetilde{\nu}_s) = (7, 0.7, 0.01)\,, \qquad \text{(C9)}$$

$$(\widetilde{m}_1, \widetilde{m}_2, \widetilde{\beta}, \widetilde{\mu}, \widetilde{\nu}_s) = \left(1.2 \times 10^3, 1 \times 10^4, 5 \times 10^2, 7 \times 10^2, 0.02\right)\,, \qquad \text{(C10)}$$

$$(\widetilde{m}_1, \widetilde{m}_2, \widetilde{\beta}, \widetilde{\mu}, \widetilde{\nu}_s) = \left(4 \times 10^2, 1 \times 10^4, 5 \times 10^2, 7 \times 10^2, 0.02\right) \qquad \text{(C11)}$$

for panels (a), (b), and (c), respectively. The patterns in Figs. 4 and 5 were obtained with model C using the parameter values in Eq. (C8). For illustration, Tables II and III provide estimates of the dimensional reaction rates implied by Eqs. (C6)–(C9) for Figs. 2, 3(a), 4, and 5 to one significant figure. The initial conditions for r and s were randomly distributed in the interval $[0, 0.01]$ and we set $(\bar{r}, \bar{s}) = (0.05, 0.05)$. We used in our simulations a grid spacing of 0.063 μm and periodic boundary conditions.

To study the sensitivity of RSD size and stability on the numerical values of our model parameters we perturbed the parameter values for model C in Eq. (C8)

TABLE III: Approximate scaffold reaction rates in Eq. (2) for various reaction schemes. All rates were estimated to one significant figure from Eqs. (C6)–(C9) and are quoted in units of s^{-1}.

Contributions to G	Model A	Model B′	Model C
$S \longrightarrow S_b$	7×10^{-1}	2×10^{-1}	5×10^{-2}
$S_b \longrightarrow S$	0	$4 \times 10^{-3}\,\overline{E}$	$3 \times 10^{-3}\,\overline{E}$
$M_b + S \longrightarrow S_b + M_b$	0	0	$8 \times 10^{-2}\,\overline{E}$
$S_b + S \longrightarrow 2S$	$7 \times 10^{-1}\overline{E}$	0	0
$S_b + 2S \longrightarrow 3S$	$2\,\overline{E}$	$3\,\overline{E}$	$2\overline{E}$

(used for Figs. 2(c), 4, and 5), and compared the resulting sizes of stable RSDs to the RSD domain size obtained with the model parameterization in Eq. (C8) (Fig. 2(c)). Our results are summarized in Fig. 6. With the exception of $\widetilde{m}_1$, we decreased or increased all model parameters by 10% relative to their values in Eq. (C8). We found that the size of RSDs depends only weakly on the value of $\widetilde{m}_1$ and, to produce an appreciable effect on domain size, we decreased $\widetilde{m}_1$ to zero and increased $\widetilde{m}_1$ to five times its value in Eq. (C8). The insensitivity of RSD size and stability on $\widetilde{m}_1$ can be understood intuitively by noting, from Eq. (B10), that $\widetilde{m}_1$ only affects the reactions $R_b \longrightarrow R$ and $M_b + R \longrightarrow M_b + R_b$ in model C which, as described above, are not crucial for the activation or inhibition of increased receptor concentrations. By contrast, Fig. 6 shows that perturbations in the value of $\widetilde{\mu}$ have the strongest effect on domain size among all model parameters. This can be intuited, from Eq. (B11), by noting that $\widetilde{\mu}$ sets the rate for the trimerization of scaffolds, $S_b + 2S \longrightarrow 3S$, which, as discussed in Sec. V, is a crucial reaction for the formation of stable RSDs by the reaction-diffusion mechanism described here.

For our simulations of pre- and postsynaptic interactions and synaptic activity we set $D_s(x, y, t) = 1$ in Figs. 4 and 5(a), and $D_r(x, y, t) = 1$ in Fig. 5(b). In Figs. 4 and 5(a) we took the function $D_r(x, y, t)$ to be a sum of Gaussians in the spatial variables with a threshold dependence on time,

$$D_r\left(\widetilde{x}, \widetilde{y}, \widetilde{t}\right) = 1 + \widetilde{A}_+ \sum_i \left\{ \theta\left(\widetilde{t} - \widetilde{t}_i\right) \theta\left(\widetilde{t}'_i - \widetilde{t}\right) \times e^{-\left[(\widetilde{x}-\widetilde{x}_i)^2 + (\widetilde{y}-\widetilde{y}_i)^2\right]/\widetilde{l}_+} \right\}, \quad \text{(C12)}$$

where $\widetilde{t}'_i > \widetilde{t}_i$ and the step function $\theta(x)$ is defined by

$$\theta(x) = \begin{cases} 1 & \text{if } x \geq 0\,, \\ 0 & \text{if } x < 0\,, \end{cases} \quad \text{(C13)}$$

with an analogous expression for $D_s(x, y, t)$ in Fig. 5(b) with $\widetilde{A}_- = -\widetilde{A}_+$. We set $\widetilde{\ell}_+ = 3$ for all the simulations shown in Figs. 4 and 5, $\widetilde{A}_+ = 1/5$ for Figs. 4(a), 4(b), and 5, and $\widetilde{A}_+ = 1/50$ for Fig. 4(c). The results displayed in Figs. 4(a) and 4(b) were obtained with $t_1 = 2.7$ hrs and $t_1 = 0$ in the limit $t'_1 \to \infty$. The values of $\widetilde{t}_i$ and $\widetilde{t}'_i$ in Figs. 4(c) and 5 were chosen as indicated in the temporal profiles of on/off stimulation. The values of the coordinates $(\widetilde{x}_i, \widetilde{y}_i)$ in Eq. (C12) were chosen to correspond to the spatial positions marked with crosses in Fig. 4. For Fig. 5, we chose the values of $(\widetilde{x}_i, \widetilde{y}_i)$ to coincide with the centers of RSDs. The qualitative behavior displayed in Figs. 4 and 5 is generic to our reaction-diffusion model, but the quantitative response of RSDs to synaptic activity depends on the details of the simulation.

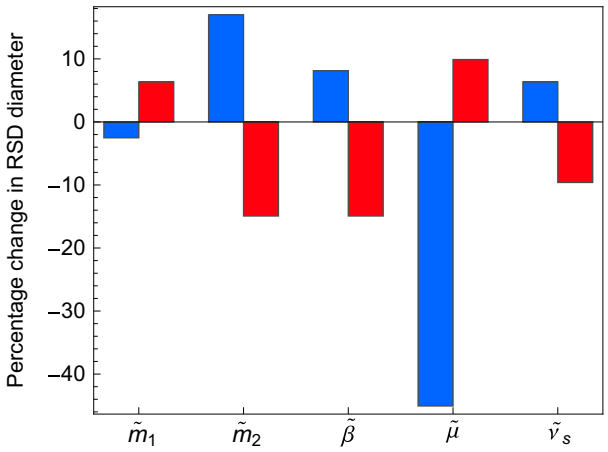

FIG. 6: (Color online) Sensitivity of RSD domain size to perturbations in model parameters. Percentage change in RSD diameter for each of the indicated model parameters, in model C, using the parameter values in Eq. (C8) as a reference model parameterization. With the exception of $\widetilde{m}_1$, all parameters were decreased (blue) or increased (red) by 10%. The parameter $\widetilde{m}_1$ was decreased to 0 (blue) and increased to five times its value in Eq. (C8) (red). The initial conditions for r and s were randomly distributed in the interval $[0, 0.1]$.

Appendix D: Extensions of the reaction-diffusion model

The reaction-diffusion model of synaptic receptor domains described in the present article is minimal, in the sense that it considers only two molecular species, receptors and scaffolds. It is also parsimonious in that it involves a small number of chemical reactions. Synaptic domains contain a large number of molecular species and involve a much longer list of chemical reactions (some of which possibly poorly described as bulk chemical reactions) [2, 4, 8, 10]. In an approach similar to the one we employed in this article, it is possible to extend the reaction-diffusion model to include alternative chemical species and additional reactions. Here, we describe some simple examples which represent mild departures from our original model and, hence, may also yield domain formation; the detailed study of these extended models lies beyond the scope of this article.

Measurements have demonstrated that (unbound) re-

ceptors can diffuse on the cellular membrane [3, 7–11, 14, 27]; by contrast, when scaffolds are transfected into a cell, they tend to gather in the cytoplasm in clumps of different sizes [26, 38]. Thus, it is possible that scaffolds cannot diffuse at the membrane if they are unbound and that receptors, effectively, 'pin' them to the membrane. In this picture, one should not consider the concentrations of unbound receptors and unbound scaffolds at the membrane as the relevant variables, but rather the concentrations of unbound receptors and bound receptor-scaffold complexes. If we assume that scaffolds are ferried from the cytoplasm to the membrane in the form of bound complexes (which is known to occur) and, conversely, that scaffolds leave the membrane also in the form of bound complexes, then the relevant models are formally identical to the models discussed in this article. Hence, patterns of stable molecular domains can also emerge spontaneously when the two interacting species are receptors and bound receptor-scaffold complexes.

The relevant models start to change, though, when we relax our fairly constraining assumptions. For example, if we allow a bound receptor-scaffold complex to unbind at the membrane, in such a way that the scaffold is reabsorbed into the cytoplasm while the receptor remains at the membrane, we obtain new reaction terms. Let us denote the concentration of bound receptor-scaffold complexes at the membrane by the symbol $\tilde{s}$. If we modify our model C minimally in order to account for our new assumptions, we obtain the reaction terms

$$F_{\tilde{s}}(r,\tilde{s}) = \underbrace{a\tilde{E}}_{R_b\longrightarrow R}\ \underbrace{-br}_{R\longrightarrow R_b}\ \underbrace{-c\tilde{E}r}_{M_b+R\longrightarrow M_b+R_b}\ \underbrace{+d\tilde{E}\tilde{s}}_{R_b+\tilde{S}\longrightarrow R+\tilde{S}}\ \underbrace{+e\tilde{E}r\tilde{s}}_{R_b+R+\tilde{S}\longrightarrow 2R+\tilde{S}}\ \underbrace{+\beta\tilde{s}}_{\tilde{S}\longrightarrow S_b}\ \underbrace{+\gamma\tilde{E}\tilde{s}}_{M_b+\tilde{S}\longrightarrow S_b+M_b}\quad , \tag{D1}$$

$$G_{\tilde{s}}(r,\tilde{s}) = \underbrace{\alpha\tilde{E}}_{\tilde{S}_b\longrightarrow\tilde{S}}\ \underbrace{-\beta\tilde{s}}_{\tilde{S}\longrightarrow S_b}\ \underbrace{-\gamma\tilde{E}\tilde{s}}_{M_b+\tilde{S}\longrightarrow S_b+M_b}\ \underbrace{+\delta\tilde{E}\tilde{s}^2}_{\tilde{S}_b+2\tilde{S}\longrightarrow 3\tilde{S}}\ , \tag{D2}$$

where $\tilde{E} = c_0 - r - \tilde{s}$ and a, b, c, d, e, α, β, γ, δ, and c_0 are constants. Chemical reactions are indicated under corresponding terms in the equations, where the symbols $\tilde{S}$ and $\tilde{S}_b$ denote bound receptor-scaffold complexes at the membrane and in the cytoplasm, respectively. The last two terms in Eq. (D1) represent the release of a receptor at the membrane from a bound receptor-scaffold complex, when the latter unbinds and its scaffold leaves the membrane. If, furthermore, unbound scaffolds reach the membrane from the cytoplasm, and *then* bind to a receptor at the membrane, the equations acquire additional terms, as

$$F'_{\tilde{s}}(r,\tilde{s}) = \underbrace{a\tilde{E}}_{R_b\longrightarrow R}\ \underbrace{-br}_{R\longrightarrow R_b}\ \underbrace{-c\tilde{E}r}_{M_b+R\longrightarrow M_b+R_b}\ \underbrace{+d\tilde{E}\tilde{s}}_{R_b+\tilde{S}\longrightarrow R+\tilde{S}}\ \underbrace{+e\tilde{E}r\tilde{s}}_{R_b+R+\tilde{S}\longrightarrow 2R+\tilde{S}}\ \underbrace{-\alpha\tilde{E}r}_{S_b\longrightarrow\tilde{S}}\ \underbrace{+\beta\tilde{s}}_{\tilde{S}\longrightarrow S_b}\ \underbrace{+\gamma\tilde{E}\tilde{s}}_{M_b+\tilde{S}\longrightarrow S_b+M_b}\ \underbrace{-\delta\tilde{E}r\tilde{s}^2}_{S_b+2\tilde{S}\longrightarrow 3\tilde{S}}\ , \tag{D3}$$

$$G_{\tilde{s}}(r,\tilde{s}) = \underbrace{\alpha\tilde{E}r}_{S_b\longrightarrow\tilde{S}}\ \underbrace{-\beta\tilde{s}}_{\tilde{S}\longrightarrow S_b}\ \underbrace{-\gamma\tilde{E}\tilde{s}}_{M_b+\tilde{S}\longrightarrow S_b+M_b}\ \underbrace{+\delta\tilde{E}r\tilde{s}^2}_{S_b+2\tilde{S}\longrightarrow 3\tilde{S}}\ . \tag{D4}$$

The last four terms in Eq. (D3) result from receptors either unbinding from bound receptor-scaffold complexes or binding to (unbound) scaffolds, at the membrane.

Analogous model variants can be formulated for the converse case, in which receptors can be found at the membrane only in their bound form, while scaffolds can be either bound or unbound. While this scenario appears to be less likely experimentally, it may be interesting on theoretical grounds. Here, in the case in which receptors arrive at the membrane in their unbound form and leave the membrane by unbinding from receptor-scaffold complexes, the reaction terms in the model variant become

$$F_{\tilde{r}}(\tilde{r},s) = \underbrace{a\tilde{E}s}_{R_b\longrightarrow\tilde{R}}\ \underbrace{-b\tilde{r}}_{\tilde{R}\longrightarrow R_b}\ \underbrace{-c\tilde{E}\tilde{r}}_{M_b+\tilde{R}\longrightarrow M_b+R_b}\ \underbrace{+e\tilde{E}\tilde{r}s}_{R_b+\tilde{R}+S\longrightarrow 2\tilde{R}+S}\quad , \tag{D5}$$

$$G_{\tilde{r}}(\tilde{r},s) = \underbrace{\alpha\tilde{E}}_{S_b\longrightarrow S}\ \underbrace{-\beta s}_{S\longrightarrow S_b}\ \underbrace{-\gamma\tilde{E}s}_{M_b+S\longrightarrow S_b+M_b}\ \underbrace{+\delta\tilde{E}rs^2}_{S_b+2S\longrightarrow 3S}\ \underbrace{-a\tilde{E}s}_{R_b\longrightarrow\tilde{R}}\ \underbrace{+b\tilde{r}}_{\tilde{R}\longrightarrow R_b}\ \underbrace{+c\tilde{E}\tilde{r}}_{M_b+\tilde{R}\longrightarrow M_b+R_b}\ \underbrace{-e\tilde{E}\tilde{r}s}_{R_b+\tilde{R}+S\longrightarrow 2\tilde{R}+S}\quad , \tag{D6}$$

where $\tilde{r}$ stands for the concentration of bound receptor-scaffold complexes, $\tilde{R}$ represents a bound receptor-scaffold complex, and, here, $\tilde{E} = c_0 - \tilde{r} - s$.

Our rationale for pointing out these 'minimal variants' of model C is that, because they are formally similar to the original model, they can be analyzed using the general framework described in the present article. More generally, however, one would like to examine models

with more than two variables. Additional variables are needed if *both* unbound *and* stable bound forms of receptors or scaffolds can be present at the membrane, and also if one is to consider other chemical species beyond receptors and scaffolds. More detailed models with a larger number of coupled equations would require an extensive study of the sort we have summarized in this article for the case of two-variable models.

[1] A. Citri and R. C. Malenka, Neuropsychopharmacology **33**, 18 (2008).
[2] P. Legendre, Cell. Mol. Life Sci. CMLS **58**, 760 (2001).
[3] C. G. Specht and A. Triller, BioEssays **30**, 1062 (2008).
[4] S. K. Tyagarajan and J.-M. Fritschy, Nat. Rev. Neurosci. **15**, 141 (2014).
[5] R. C. Carroll, E. C. Beattie, M. von Zastrow, and R. C. Malenka, Nat. Rev. Neurosci. **2**, 315 (2001).
[6] J. D. Shepherd and R. L. Huganir, Ann. Rev. Cell Dev. Biol. **23**, 613 (2007).
[7] M. Kneussel, A. Triller, and D. Choquet, Cell **157**, 1738 (2014).
[8] D. Choquet and A. Triller, Neuron **80**, 691 (2013).
[9] D. Choquet and A. Triller, Nat. Rev. Neurosci. **4**, 251 (2003).
[10] A. Triller and D. Choquet, Neuron **59**, 359 (2008).
[11] A. Triller and D. Choquet, Trends Neurosci. **28**, 133 (2005).
[12] S. Okabe, H.-D. Kim, A. Miwa, T. Kuriu, and H. Okado, Nat. Neurosci. **2**, 804 (1999).
[13] N. W. Gray, R. M. Weimer, B. I., and K. Svoboda, PLoS Biol. **4**, 2065 (2006).
[14] M. Calamai, C. G. Specht, J. Heller, D. Alcor, P. Machado, C. Vannier, and A. Triller, J. Neurosci. **29**, 7639 (2009).
[15] N. E. Ziv and A. Fisher-Lavie, Neuroscientist **20**, 439 (2014).
[16] J. T. Trachtenberg, B. E. Chen, G. W. Knott, G. Feng, J. R. Sanes, E. Welker, and K. Svoboda, Nature **420**, 788 (2002).
[17] J. Grutzendler, N. Kasthuri, and W.-B. Gan, Nature **420**, 812 (2002).
[18] F. Crick, Nature **312**, 101 (1984).
[19] H. Z. Shouval, Proc. Natl. Acad. Sci. U.S.A. **102**, 14440 (2005).
[20] K. Sekimoto and A. Triller, Phys. Rev. E **79**, 031905 (2009).
[21] D. Holcman and A. Triller, Biophys. J. **91**, 2405 (2006).
[22] V. M. Burlakov, N. Emptage, A. Goriely, and P. C. Bressloff, Phys. Rev. Lett. **108**, 028101 (2012).
[23] B. A. Earnshaw and P. C. Bressloff, J. Neurosci. **26**, 12362 (2006).
[24] K. Czöndör, M. Mondin, M. Garcia, M. Heine, R. Frischknecht, D. Choquet, J.-B. Sibarita, and O. R. Thoumine, Proc. Natl. Acad. Sci. U.S.A. **109**, 3522 (2012).
[25] A. K. McAllister, Ann. Rev. Neurosci. **30**, 425 (2007).
[26] J. Meier, C. Meunier-Durmont, C. Forest, A. Triller, and C. Vannier, J. Cell Sci. **113**, 2783 (2000).
[27] J. Meier, C. Vannier, A. Sergé, A. Triller, and D. Choquet, Nat. Neurosci. **4**, 253 (2001).
[28] M. Dahan, S. Lévi, C. Luccardini, P. Rostaing, B. Riveau, and A. Triller, Science **302**, 442 (2003).
[29] C. A. Haselwandter, M. Calamai, M. Kardar, A. Triller, and R. A. da Silveira, Phys. Rev. Lett. **106**, 238104 (2011).
[30] J. R. Sanes and J. W. Lichtman, Nat. Rev. Neurosci. **2**, 791 (2001).
[31] M. J. Anderson and J. Cohen, J. Physiol. **268**, 757 (1977).
[32] E. Frank and G. D. Fischbach, J. Cell Biol. **83**, 143 (1979).
[33] T. Misgeld, R. W. Burgess, R. M. Lewis, J. M. Cunningham, J. W. Lichtman, and J. R. Sanes, Neuron **36**, 635 (2002).
[34] H. Flanagan-Steet, M. A. Fox, D. Meyer, and J. R. Sanes, Development **132**, 4471 (2005).
[35] J. A. Panzer, S. M. Gibbs, R. Dosch, D. Wagner, M. C. Mullins, M. Granato, and R. J. Balice-Gordon, Dev. Biol. **285**, 340 (2005).
[36] T. T. Kummer, T. Misgeld, and J. R. Sanes, Curr. Opin. Neurobiol. **16**, 74 (2006).
[37] C. Hanus, M.-V. Ehrensperger, and A. Triller, J. Neurosci. **26**, 4586 (2006).
[38] J. Kirsch, J. Kuhse, and H. Betz, Mol. Cell. Neurosci. **6**, 450 (1995).
[39] A. M. Turing, Phil. Trans. B **237**, 37 (1952).
[40] I. R. Epstein and J. A. Pojman, *An Introduction to Nonlinear Chemical Dynamics* (Oxford University Press, New York, 1998).
[41] D. Walgraef, *Spatio-Temporal Pattern Formation* (Springer-Verlag, New York, 1997).
[42] M. Cross and H. Greenside, *Pattern Formation and Dynamics in Nonequilibrium Systems* (Cambridge University Press, Cambridge, 2009).
[43] M. C. Cross and P. C. Hohenberg, Rev. Mod. Phys. **65**, 851 (1993).
[44] A. Gierer and H. Meinhard, Kybernetik **12**, 30 (1972).
[45] J. D. Murray, *Mathematical Biology* (Springer-Verlag, Berlin and Heidelberg, 2002), 3rd ed.
[46] H. Meinhardt, *Models of Biological Pattern Formation* (Academic Press, London, 1982).
[47] P. K. Maini and H. G. Othmer, eds., *Mathematical Models for Biological Pattern Formation* (Springer-Verlag, New York, 2001).
[48] M. Irie, Y. Hata, M. Takeuchi, K. Ichtchenko, A. Toyoda, K. Hirao, Y. Takai, T. W. Rosahl, and T. C. Südhof, Science **277**, 1511 (1997).
[49] J.-Y. Song, K. Ichtchenko, T. C. Südhof, and N. Brose, Proc. Natl. Acad. Sci. U.S.A. **96**, 1100 (1999).
[50] N. K. Hussain and M. Sheng, Science **307**, 1207 (2005).
[51] B. Chih, H. Engelman, and P. Scheiffele, Science **307**, 1324 (2005).
[52] C. Dean and T. Dresbach, Trends Neurosci. **29**, 21 (2006).
[53] C. Tardin, L. Cognet, C. Bats, B. Lounis, and D. Choquet, EMBO J. **22**, 4656 (2003).
[54] S. Lévi, C. Schweizer, H. Bannai, O. Pascual, C. Charrier, and A. Triller, Neuron **59**, 1 (2008).
[55] H. Bannai, S. Lévi, C. Schweizer, T. Inoue, T. Launey,

V. Racine, J.-B. Sibarita, K. Mikoshiba, and A. Triller, Neuron **62**, 670 (2009).
[56] C. A. Lugo and A. J. McKane, Phys. Rev. E **78**, 051911 (2008).
[57] A. J. McKane and T. J. Newman, Phys. Rev. E **70**, 041902 (2004).
[58] J. E. Satulovsky, J. Theor. Biol. **183**, 381 (1996).
[59] I. L. Novak, B. M. Slepchenko, A. Mogilner, and L. M. Loew, Phys. Rev. Lett. **93**, 268109 (2004).
[60] S. Kondo and T. Miura, Science **329**, 1616 (2010).
[61] J. Howard, S. W. Grill, and J. S. Bois, Nat. Rev. Mol. Cell Biol. **12**, 392 (2011).
[62] S. Butz, M. Okamoto, and T. C. Südhof, Cell **94**, 773 (1998).
[63] E. Yeramian and J.-P. Changeux, C. R. Acad. Sc. Paris **302**, 609 (1986).
[64] J. Reinitz, Nature **482**, 464 (2012).
[65] P. K. Maini, Proc. Natl. Acad. Sci. U.S.A. **100**, 9656 (2003).
[66] N. Suzuki, M. Hirata, and S. Kondo, Proc. Natl. Acad. Sci. U.S.A. **100**, 9680 (2003).
[67] P. K. Maini, R. E. Baker, and C.-M. Chuong, Science **314**, 1397 (2006).
[68] S. Sick, S. Reinker, J. Trimmer, and T. Schlake, Science **314**, 1447 (2006).
[69] L. Wolpert, J. Theor. Biol. **25**, 1 (1969).
[70] M. Howard, A. D. Rutenberg, and S. de Vet, Phys. Rev. Lett. **87**, 278102 (2001).
[71] H. Meinhardt and P. A. J. de Boer, Proc. Natl. Acad. Sci. U.S.A. **98**, 14202 (2001).
[72] K. C. Huang, Y. Meir, and N. S. Wingreen, Proc. Natl. Acad. Sci. U.S.A. **100**, 12724 (2003).
[73] R. V. Kulkarni, K. C. Huang, M. Kloster, and N. S. Wingreen, Phys. Rev. Lett. **93**, 228103 (2004).
[74] L. Rothfield, A. Taghbalout, and Y.-L. Shih, Nat. Rev. Microbiol. **3**, 959 (2005).
[75] K. Kruse, M. Howard, and W. Margolin, Mol. Microbiol. **63**, 1279 (2007).
[76] J. Lutkenhaus, Annu. Rev. Biochem. **76**, 539 (2007).
[77] M. Loose, E. Fischer-Friedrich, J. Ries, K. Kruse, and P. Schwille, Science **320**, 789 (2008).
[78] J. Kirsch, I. Wolters, A. Triller, and H. Betz, Nature **366**, 745 (1993).
[79] C. Béchade, I. Colin, J. Kirsch, H. Betz, and A. Triller, Eur. J. Neurosci. **8**, 429 (1996).
[80] C. M. McCann, J. C. Tapia, H. Kim, J. S. Coggan, and J. W. Lichtman, Nat. Neurosci. **11**, 807 (2008).
[81] G. Strobl, *The Physics of Polymers* (Springer-Verlag, Berlin, 2006), 3rd ed.
[82] A. Gamba, I. Kolokolov, V. Lebedev, and G. Ortenzi, Phys. Rev. Lett. **99**, 158101 (2007).
[83] T. Butler and N. Goldenfeld, Phys. Rev. E **80**, 030902 (2009).
[84] T. Butler and N. Goldenfeld, Phys. Rev. E **84**, 011112 (2011).
[85] N. G. van Kampen, *Stochastic Processes in Physics and Chemistry* (North-Holland, Amsterdam, 1992), 2nd ed.
[86] C. A. Haselwandter and D. D. Vvedensky, Phys. Rev. E **76**, 041115 (2007).
[87] R. F. Fox and J. Keizer, Phys. Rev. A **43**, 1709 (1991).
[88] W. Horsthemke and L. Brenig, Z. Phys. B **27**, 341 (1977).
[89] C. A. Haselwandter and D. D. Vvedensky, J. Phys. A: Math. Gen. **35**, L579 (2002).
[90] S. Hanna, W. Hess, and R. Klein, Physica A: Stat. Mech. Appl. **111**, 181 (1982).
[91] J. Sun and H. Weinstein, J. Chem. Phys. **127**, 155105 (2007).
[92] D. T. Gillespie, J. Comput. Phys. **22**, 403 (1976).
[93] D. T. Gillespie, J. Phys. Chem. **81**, 2340 (1977).